



**HAL**  
open science

## Early, far-field and diffuse tectonics records in the North Aquitaine Basin (France)

Loïc Bouat, Pierre Strzeczynski, Régis Mourgues, Yannick Branquet, Nathan Cogné, Guillaume Barré, Véronique Gardien

► **To cite this version:**

Loïc Bouat, Pierre Strzeczynski, Régis Mourgues, Yannick Branquet, Nathan Cogné, et al.. Early, far-field and diffuse tectonics records in the North Aquitaine Basin (France). Bulletin de la Société Géologique de France, 2023, 194, pp.17. 10.1051/bsgf/2023014 . insu-04224441v2

**HAL Id: insu-04224441**

**<https://insu.hal.science/insu-04224441v2>**

Submitted on 20 Dec 2023

**HAL** is a multi-disciplinary open access archive for the deposit and dissemination of scientific research documents, whether they are published or not. The documents may come from teaching and research institutions in France or abroad, or from public or private research centers.

L'archive ouverte pluridisciplinaire **HAL**, est destinée au dépôt et à la diffusion de documents scientifiques de niveau recherche, publiés ou non, émanant des établissements d'enseignement et de recherche français ou étrangers, des laboratoires publics ou privés.



Distributed under a Creative Commons Attribution 4.0 International License

## Early, far-field and diffuse tectonics records in the North Aquitaine Basin (France)

Loïc Bouat<sup>1,\*</sup>, Pierre Strzeczynski<sup>1</sup>, Régis Mourgues<sup>1</sup>, Yannick Branquet<sup>2,3</sup>, Nathan Cogné<sup>2</sup>, Guillaume Barré<sup>4</sup> and Véronique Gardien<sup>5</sup>

<sup>1</sup> Laboratoire de Planétologie et Géodynamique, UMR6112, CNRS, Le Mans Université, France

<sup>2</sup> Géosciences Rennes, UMR6118, CNRS Université de Rennes, France

<sup>3</sup> Institut des Sciences de la Terre d'Orléans, UMR7237, CNRS, Université d'Orléans, France

<sup>4</sup> Département de géologie et génie géologique, Centre E4M, Université Laval, Canada

<sup>5</sup> Laboratoire de Géologie de Lyon, UMR5276, CNRS, Université Lyon 1, France

Received: 15 December 2022 / Accepted: 26 September 2023 / Publishing online: 20 December 2023

**Abstract** – In Western Europe, the deformations related to the opening of the Bay of Biscay and the formation of the Pyrenean belt are well described in the southern part of the Aquitaine Basin, but little is known about the impact of these geodynamic events towards the Northern Aquitaine Platform. In this paper, we combine field observation with Unmanned Aerial Vehicle (UAV) imagery and calcite U-Pb geochronology to determine precisely the tectonic evolution in the Vendée Coastal domain. We evidence two main tectonic events: (1) At the transition between the Late Jurassic to Early Cretaceous, WNW-ESE striking normal faults formed horsts and grabens at the onset of the opening of the Bay of Biscay. The reactivation of Variscan faults during this tectonic event is consistent with oblique extension. This event triggered ascending fluid flows that mix with Basin fluids responsible for barite-pyrite-quartz mineralizations near the unconformity. (2) During the Late Cretaceous, fractures, wide-open folds, veins, and joints are consistent with the N-S shortening direction during the earliest stages of the Pyrenean compression.

In both cases, the Northern Aquitaine Platform records the early stages of the main regional tectonic events in a far-field position. In the northern Aquitaine Basin, as in many other places in Europe, the tectonic study of sedimentary platforms located far from the plate boundaries provides new constraints on the early diffuse deformation process that predate the main tectonic phases.

**Keywords:** Intraplate deformation / calcite U-Pb geochronology / Northern Aquitaine platform / Biscay Bay / Pyrenees / U.A.V. imaging

### Résumé – Enregistrements tectoniques précoces, lointains et diffus dans le Nord du Bassin aquitain. Résumé

Au cours des périodes du Mésozoïque et du Cénozoïque, l'Europe a connu plusieurs événements tectoniques interprétés comme de la tectonique lointaine. Il peut s'agir d'une tectonique diffuse qui se produit au début d'un événement tectonique majeur ou de la propagation au loin de la déformation des fronts orogéniques. En Europe de l'Ouest, les déformations liées à l'ouverture du Golfe de Gascogne et à la formation de la chaîne des Pyrénées sont bien décrites dans le sud du Bassin aquitain, là où la plate-forme Nord aquitaine reste peu étudiée. Nous avons combiné les observations de terrain, l'imagerie par drone et la datation laser U-Pb sur la calcite pour déterminer l'évolution tectonique du domaine côtier de la Vendée. Nos résultats mettent en évidence l'existence de deux événements tectoniques majeurs depuis le début du Jurassique : (1) À la transition du Jurassique supérieur au Crétacé inférieur, des failles normales orientées ONO-ESE présentent une organisation en hosts et grabens au début de l'ouverture du Golfe de Gascogne. Leur association avec des failles décrochantes varisques réactivées est cohérente avec une organisation oblique de l'extension. Cet événement tectonique est accompagné par la circulation d'un fluide profond. (2) Durant le Crétacé supérieur, la mise en place de fractures, de plis ouverts, de veines et de joints est cohérent avec la direction de

\*Corresponding author: [loic.bouat@univ-lemans.fr](mailto:loic.bouat@univ-lemans.fr)

raccourcissement N-S qui se produit au premiers stades de la compression N-S des Pyrénées. Dans les deux cas, les premiers stades des principaux épisodes de déformation régionale ont été enregistrés par une tectonique lointaine sur la plateforme Nord aquitaine, avant la localisation de la déformation dans les rifts et dans les Pyrénées. Dans le Bassin aquitain, comme dans de nombreux endroits en Europe, l'étude tectonique des plates-formes sédimentaires situées loin des zones principales de déformation à l'échelle des plaques apporte de nouvelles contraintes sur les processus de déformations précoces et diffus antérieurs aux principales phases tectoniques.

**Mots clés :** Déformation intraplaque / tectonique précoce et diffuse / déformation lointaine / géochronologie U-Pb sur calcite / plateforme Nord Aquitaine / Golfe de Gascogne / Pyrénées

## 1 Introduction

The plate tectonics theory defines lithospheric plates as rigid blocks bounded by deformable boundaries (McKenzie and Parker, 1967). However, numerous observations have evidenced intra-plate deformations, also called “far-field deformations” (e.g., Ziegler *et al.*, 1995). Within the Basin, intra-plate deformations induce burial or uplift, hydrocarbon maturation, fluid flow changes, and mineral depositions (Boiron *et al.*, 2010; Burisch *et al.*, 2022; Gorczyk *et al.*, 2013; Turner and Williams, 2004).

Far-field deformations occurred in divergence and convergence contexts, and their timing relative to rifting or mountain building is variable. In the divergence context, diffuse extensions predating strain localization within rifts are highlighted by uplift, tectonic reactivation, and fracture networks formation (Huerta and Harry, 2007; Seymour *et al.*, 2016; Szymanski *et al.*, 2016). However, this strain focusing within rifts is sometimes counterbalanced by the activation of several décollement levels in the context of multilayered lithosphere leading the deformation to propagate far from the main thinning zone (Clerc *et al.*, 2016; Lagabrielle *et al.*, 2020; Dhifaoui *et al.*, 2021). In a convergence context, intra-plate deformations occur during orogenic processes several hundred kilometers away from the mountain belt front (Jolivet *et al.*, 2021; Lacombe & Mouthereau, 1999). They are accompanied by uplifting following lithospheric folding (Gerbault *et al.*, 1999; Ziegler *et al.*, 1995), tectonic reactivation (Gorczyk *et al.*, 2013; Navabpour *et al.*, 2017; Parizot *et al.*, 2022), and the formation of new fault and joint networks (Duperret *et al.*, 2012; Missenard *et al.*, 2017). However, far-field deformation takes place sometimes at the onset of convergence resulting in the inversion of pre-existing structures such as rift (Frizon *et al.*, 2000) or passive margins (Leffondré *et al.*, 2021, Strzeczynski *et al.*, 2021;) and in the folding of the lithosphere (Cloetingh and Burov, 2011). Whatever the tectonic context, far-field deformation is always linked with vertical motion, tectonic reactivation of basement structure, and fracture network formation.

In Western Europe, two periods are particularly suitable for intra-plate tectonics: 1) the Late Jurassic to early Cretaceous, in a framework of extensional tectonics, which relates to the opening of the North Atlantic Ocean (Ziegler, 1990; Ziegler and Dèzès, 2005). In the Aquitaine Basin, deformation is concentrated on a limited area between the Celtaquitaine flexure in the north and the North Pyrenean Fault in the south (Fig. 1; BRGM and Esso-Rep, 1974; Jammes *et al.*, 2009; Issautier *et al.*, 2022; Tugend *et al.*, 2014) suggesting that no diffuse extension is recorded. However, it has also been

proposed that the early deformations were not focused and extended north of the Celtaquitaine flexure (Asti *et al.*, 2022). 2) The period from the Late Cretaceous to Eocene, in a setting of coeval compression, related to the Pyrenees orogeny. Late Cretaceous to Eocene intra-plate deformation is particularly well described in Iberia (De Ruig *et al.*, 1990), in the Paris Basin (Blaise *et al.*, 2022; Lacombe and Obert, 2000; Lacombe *et al.*, 1990), southern England (Duperret *et al.*, 2012; Parrish *et al.*, 2018) and the North sea and Central Europe (Dielforder *et al.*, 2019; Evans *et al.*, 2003).

The North Aquitaine Platform is located along the western coast of France, at 100 and 300km north of the Bay of Biscay and Pyrenees front, respectively (Fig. 1). Here, geophysical investigations point to the absence of large-scale deformation, such as rifts or inverted structures (Bois *et al.*, 1997; Jammes *et al.*, 2009). However, at the outcrop scale, several deformation phases have been described, but no consensus exist: For some authors (Burbaud-Vergneaud, 1987; Bouton and Branger *et al.*, 2007), no tectonic events occurred during the Mesozoic and at least six deformation episodes take place during the Cenozoic. Their timings are only constrained by the analogy of the stress direction with the peri-alpine domain (Bergerat, 1987). For others (Cathelineau *et al.*, 2012, Strzeczynski *et al.*, 2020), normal faults crossing the first Mesozoic sedimentary formation are associated with fluid circulation and mineral deposition. Here, the timing of faulting is indirectly constrained by the datation of the basement alteration and adularization, in a possible relationship with fluid circulation and mineral deposition (Cathelineau *et al.*, 2012). No direct time constraints are available on the Mesozoic to Present tectonic event of the North Aquitaine Platform. No studies encompass the relationship between brittle deformation in the basement units and the sedimentary cover.

The following paper provides new structural and time constraints on North Aquitaine Platform to constrain far-field tectonics in this area and better understand how this can modify the fluid pathways and impact mineral deposition. We especially focused on the criteria characterizing the far-field deformation without a large-scale structure, such as tectonic reactivation of basement structure and fracture network formation. We conducted a geological study across the unconformity that separates the Armorican basement and the Aquitaine Basin. The exceptional outcrop conditions of the Vendée coast allow us to perform a structural survey based on detailed maps assisted by Unmanned Aerial Vehicle (UAV). In addition, we provide new time constrain on the syn-kinematic mineral by direct dating of calcite filling fractures using Laser ablation ICP-MS U-Pb geochronology. Then, we discuss the relationships between outcrop scale deformations and the main

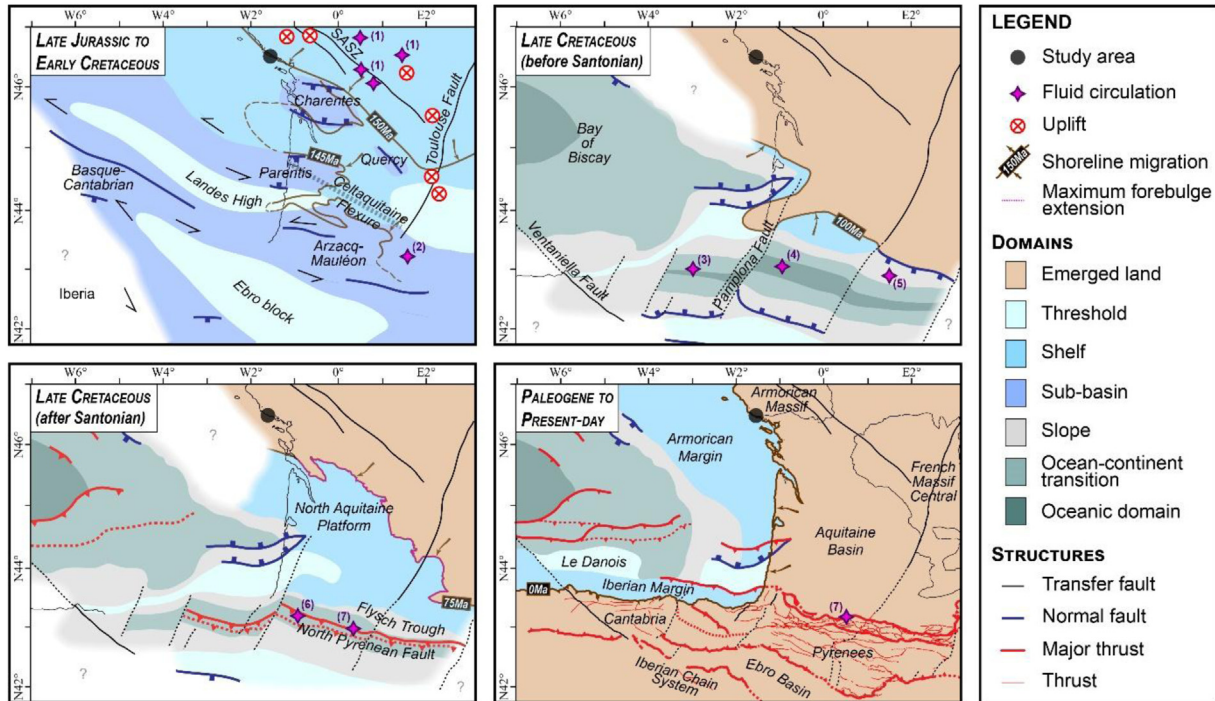


**Fig. 1.** Iberian-European plate boundary reconstitution from Jurassic-Cretaceous transition through present-day (spatial and temporal restoration map modified from Tugend *et al.* (2015) with data from Asti *et al.* (2022), Biteau *et al.* (2006) and Thomas *et al.* (1996); fluid circulation reports from (1) Cathelineau *et al.* (2012); (2) Munoz *et al.* (2016); (3) DeFelipe *et al.* (2017); (4) Corre *et al.* (2018), Incerpi *et al.* (2020), Salardon *et al.* (2017); (5) Boutin *et al.* (2016), Quesnel *et al.* (2019); (6) Salardon *et al.* (2017); (7) Barré *et al.* (2021); uplift movement from thermochronology studies of Barbarand *et al.* (2020) and François *et al.*, (2020); maximum fore bulge extension from Angrand *et al.* (2018)). S.A.S.Z.: South Armorian Shear Zone.

tectonic events of the Aquitaine Basin, such as the Bay of Biscay opening and the Pyrenean orogeny.

## 2 Geological setting

The Mesozoic North Aquitaine Platform emplaced over the Armorican basement that well recorded the latest stage of the Variscan evolution (Ballèvre *et al.*, 2009; Cagnard *et al.*, 2004; Gapais *et al.*, 2015; Goujou *et al.*, 1994). The latter is characterized by HT-LP metamorphism in a WNW-ESE extension context (Cagnard *et al.*, 2004; Goujou *et al.*, 1994; Iglésias and Brun, 1976) and that has been dated further north at ca. 320 Ma (Augier *et al.*, 2015; Turrillot *et al.*, 2011). The Armorican basement consists of migmatitic gneiss at the Anse aux Moines, kyanite and sillimanite bearing gneiss that is intruded by aplo-pegmatitic dikes in Cayola Bay and kyanite micaschists in Mine des Sardes and Anse de Saint-Nicolas (Fig. 2). Such a distribution of metamorphic rocks is consistent with a decrease of Barrovian-type metamorphism from the N. W. to the S.E., as proposed by Goujou *et al.*, (1994). Ductile structures associated with this metamorphism gradually evolve into brittle structures such as N-S normal faults and a large shear zone at ca. 300 Ma (Turrillot *et al.*, 2011).

Erosion and peneplanation occurring during the Late Paleozoic to Triassic periods are responsible for the continued exhumation of the basement rocks. At the end of the Jurassic, the Armorican basement from Vendée was buried under a thick layer (~1 km) of platform sediments, causing a maximum

temperature rise of 60 °C at the bottom of the Basin (François *et al.*, 2020).

Fluid flows, inducing authigenic minerals precipitation near faults and along sedimentary strata, occurred during the Jurassic – Cretaceous transition as attested by  $^{40}\text{Ar}/^{39}\text{Ar}$  and K-Ar dating on adularia and clays (illite, smectite, and kaolinite) of Cathelineau *et al.* (2012), in an N-S extensional setting (Strzeczynski *et al.*, 2020). The numerous normal faults of the Aquitaine Mesozoic units are successively filled by barite, pyrite, quartz, or calcite (Fig. 2c; Strzeczynski *et al.*, 2020). Fluids responsible for mineral deposition have variable temperatures and salinities, suggesting different fluid sources from secondary brines such as the Basin and sea water mixed with rising warm water (Cathelineau *et al.*, 2012). The latter is particularly important along the Vendée coast north of the Aquitaine Basin, as evidenced by the high fluid temperatures (Cathelineau *et al.*, 2012).

These fluid circulations and the associated tectonic event coincide with a major marine regression that induces the emersion of the North Aquitaine Platform in the Early Cretaceous (Fig. 1; Biteau *et al.*, 2006; B.R.G.M., 1974; Curnelle and Dubois, 1986). At that time, the Variscan basement rocks begin to exhume due to the erosion of the Aquitaine Basin sedimentary cover (François *et al.*, 2020). Exhumation is relatively fast as the basement rocks have been near the surface since Cretaceous times (François *et al.*, 2020). Cenozoic structures have been dated by the relationship between continental deposits and regional tectonic (Burbaud-

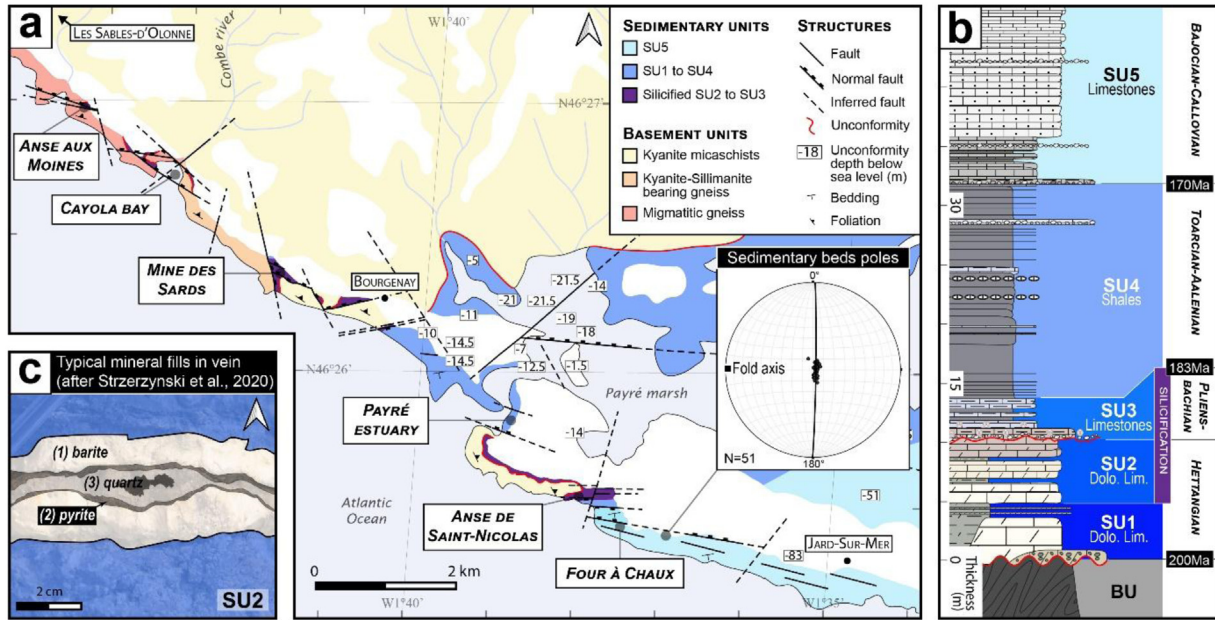


**Fig. 2.** (a) Geological map of the Vendée coastal domain modified after [Ters and Gabilly \(1986\)](#) based on field observations with close attention on faults shifting the unconformity and unconformity depth (B.S.L.: Below Sea Level) compiled after B.R.G.M. database ([B.S.S. n.d.](#)). (b) Simplified geological log from [Strzeczynski et al. \(2020\)](#). Dolo. Lim.: Dolomitic limestones (c) Pattern of vein paragenesis after [Strzeczynski et al. \(2020\)](#).

[Vergneaud, 1987](#); [Bouton and Branger et al., 2007](#)). It attests to (i) N-S shortening in the Eocene, consistent with Pyrenean orogeny, (ii) an NNE-SSW extension in the Oligocene, compatible with the European Cenozoic rift system ([Ziegler and Dèzes, 2005](#)), followed by (iii) an E-W shortening in the Miocene and (iv) an NW-SE shortening from the Pliocene to the present day, which may relate to the Alpine orogeny ([Bergerat, 1987](#)).

### 3 Methods

Our approach is based on three main steps: 1) structural characterization. Thanks to excellent outcrop conditions on the rocky coastal plateau, we propose detailed structural maps constrained by UAV imagery coupled with orientation and length measurements of the structure. 2) relative chronology based on cross-sectional relationships of structural maps, and 3) absolute dating of authigenic minerals.

#### 3.1 Structure characterization

The study focuses on fractures, a group of structures encompassing joints and faults ([Peacock et al., 2016](#)). Joints are characterized by opening from either side of the fracture (rupture mode I), and faults are associated with movement in the same direction as the fracture (rupture mode II) ([Pollard and Aydin, 1988](#)). Fractures can be filled by minerals that form veins and slickensides in the case of mode I openings and mode II slips, respectively ([Bons et al., 2012](#)).

We systematically measured the structure's strike, dip, and dip direction in the field with a compass and reported mineral fills (G.P.S. coordinates and sampling).

#### 3.2 UAV imagery

UAV imagery was deployed in all areas on the tidal rocky shelf. The UAV is a DJI Phantom 4 equipped with a 12 Mpixels camera. Picture acquisition was made at an altitude of 70 m. Then, photographs were merged into four high-resolution orthomosaics. The spatial resolution is 30 × 30 mm/pixel.

We provide a high-resolution geological map of the tidal rocky shelf by manually digitizing fractures and remarkable levels under the G.I.S. environment (QGIS 3.16 software). We selected fractures at least 10 m long for better clarity on high-resolution geological maps. Indeed, shorter fractures could be the response to rearrangement with little deviation due to a small-scale stress field. Strike and length were calculated from fractures traces in Q.G.I.S., and length-weighted rose diagrams were produced by multiplying the number of each fracture measurement by its length (for example, an N90° striking fracture of 3m long is considered as “N90; N90; N90” in the rose diagram). Length-weighted rose diagrams were displayed with GeoRose 0.5.1 software.

#### 3.3 Relative chronology

The relative chronology between fractures is based on three topological relationships ([Fig. 3](#); [Sanderson and Nixon, 2015](#)): isolated, intersecting, and abutting fracture terminations. Isolated

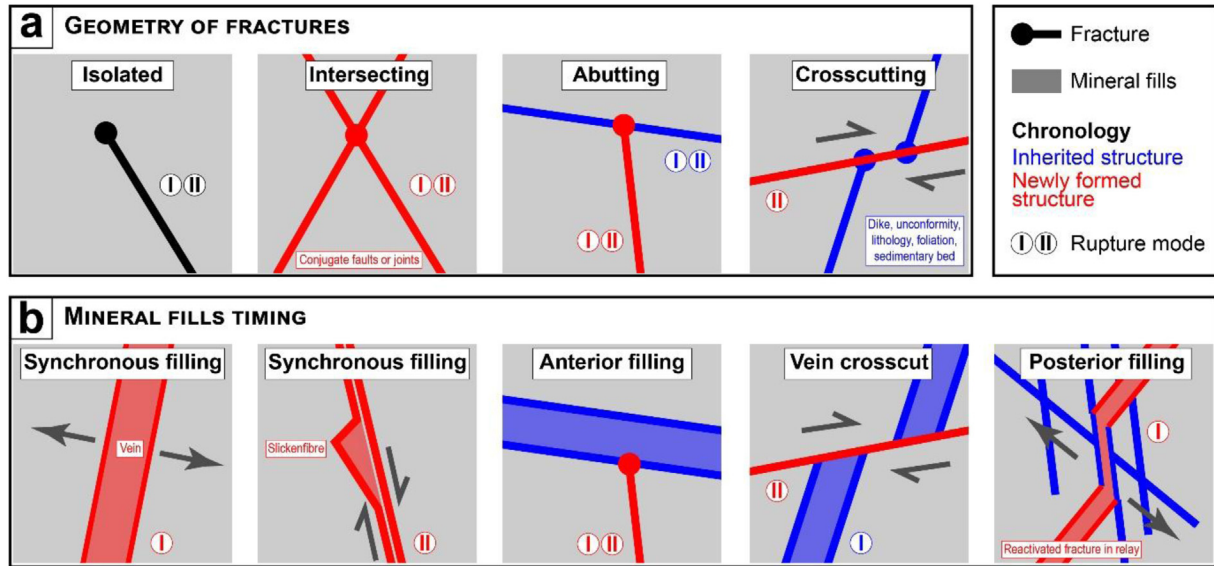


**Fig. 3.** Relative chronology of structure and mineral fills (after [Bons \*et al.\* \(2012\)](#), [Sanderson and Nixon \(2015\)](#), and [Peacock \*et al.\* \(2016\)](#)). (a) The geometry of fractures and their chronology with their rupture mode. (b) Mineral fills timing concerning fractures depending on their rupture mode.

fracture terminations, with an “I” geometry and “X” shape intersection without mineral fillings, don’t allow a precise relative chronology to be obtained. If the fractures have an “X” shape intersection that could form under the same stress field and for faults opposite shear senses, in that case, they are considered synchronous as conjugated fractures ([Anderson, 1951](#); [Daubrée, 1878](#); cited by [Dennis, 1967](#)). Abutment geometry refers to a “T” shape geometry with one fracture stopping against another, meaning it terminates against a pre-existing fracture ([Sanderson and Nixon, 2015](#)).

Mineral precipitation could be synchronous, anterior, or posterior to the fractures ([Fig. 3](#)). Synchronous mineral fills joints, veins, and slickenfibres on fault planes ([Bons \*et al.\*, 2012](#)). Except for slickenfibres, other observations, such as the mineral texture and microstructure, help to decipher the synchronicity of the mineral filling. If the duration between fault activity and mineral precipitation is smaller than the dating uncertainties, they are interpreted as synchronous ([Roberts and Holdsworth, 2022](#)). Anterior mineral fillings in a new fracture are interpretable with an abutment or crosscutting geometry on the anterior mineral filling. The late mineral filling requires additional chronological evidence, such as a crosscutting relationship with other geological features, to be distinguished from synchronous mineral fillings. In all cases, inherited fractures that reopen by forming veins do not open in type I mode and have an oblique component ([Fig. 3](#)). They act as a relay structure between newly formed veins ([Virgo \*et al.\*, 2014](#)) unless there is a separate tectonic event with the same stress field, which is unlikely.

### 3.4 Calcite U-Pb geochronology

We selected calcite samples from veins with a clear orientation and chronology. The selected calcite samples comprise rhombohedral blocky crystals 0.5 to 3 cm wide.

Individual calcite crystals from the three samples were hand-picked and polished in an epoxy mount. They were imaged using cold cathodoluminescence, and no zoning was observed. U-Pb analyses on calcite were performed at the Plateforme GeOHeLiS, Géosciences Rennes (Université de Rennes) using an ESI NWR193UC Excimer laser coupled to an Agilent 7700x, Q-ICP-MS equipped with a dual pumping system to enhance sensitivity. Ablation spots of 100  $\mu\text{m}$  diameter with a repetition rate of 10 Hz and a fluence of 6 J/cm<sup>2</sup> were used. The general protocol follows the one in [Coltat \*et al.\* \(2019\)](#) and is fully described in the Supplementary data with the instrumental condition table. WC1 ([Roberts \*et al.\*, 2017](#)) is the primary reference material. Data reduction was performed with Iolite v4 software ([Paton \*et al.\*, 2011](#)) using U-Pb VizualAge UComPbine D.R.S. ([Chew \*et al.\*, 2014](#)). Sample age calculations and Tera-Wasserburg diagrams were made using IsoplotR ([Vermeesch, 2018](#)). All uncertainties are quoted at the  $2\sigma$  level. Propagation of excess scatter on primary R.M. is propagated to individual ratio measurements. Systematic uncertainty on the ratios of primary R.M. and decay constants uncertainties are propagated to the final age calculation. Propagation is made by quadratic addition following [Horstwood \*et al.\* \(2016\)](#).

## 4 Results

The field observations assisted by UAV imaging of the different lithologies and the brittle structure are obtained on six outcrops along the Vendée Coast from northwest to southeast ([Fig. 2](#)) as follows: the Anse aux Moines ([Fig. 4](#)), the Cayola Bay ([Fig. 5](#)), the Mine des Sardes ([Fig. 6](#)), the Payré Estuary ([Fig. 7](#)), the Anse de Saint-Nicolas ([Fig. 8](#)) and Four à Chauv ([Fig. 9](#)).

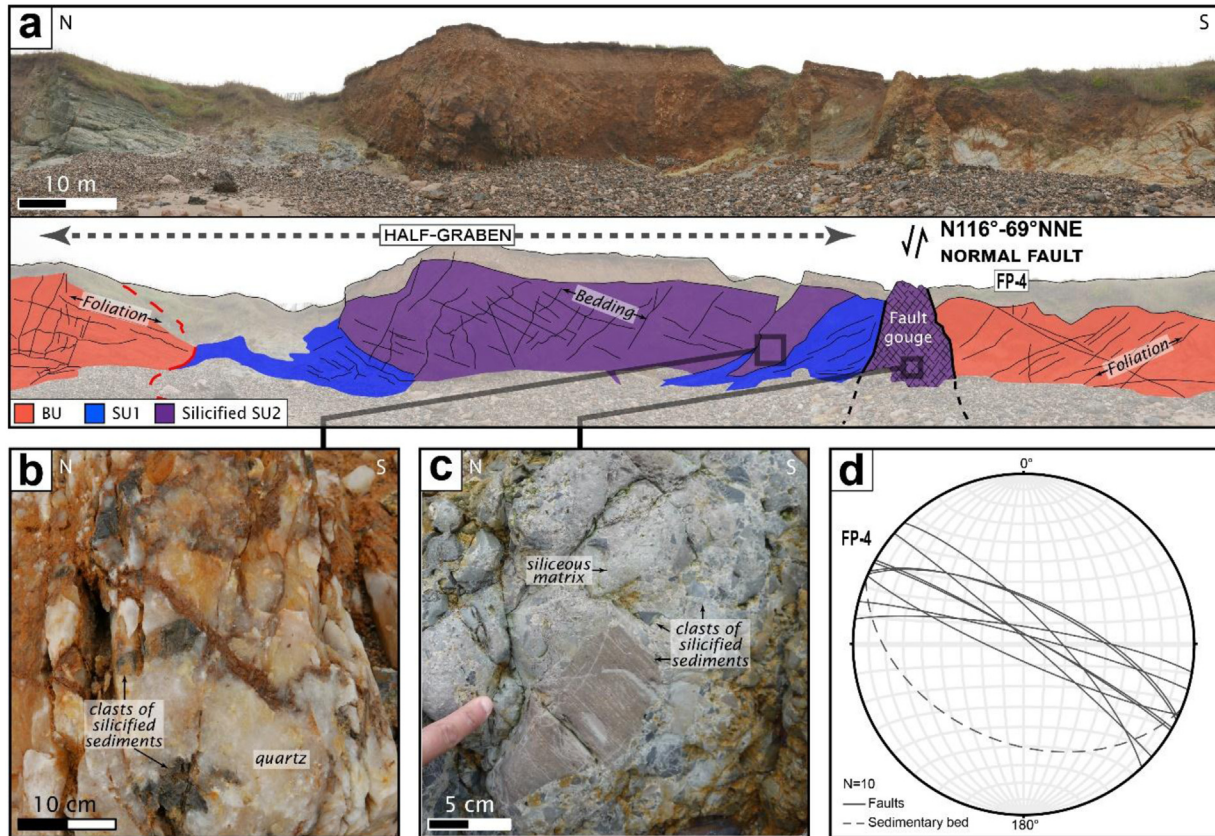


**Fig. 4.** Anse aux Moines coastal cliff. (a) Composite picture and structural interpretation of the coastal cliff limited to the south by a normal fault that shifts the unconformity and tilts SU1 and SU2 beddings to the south. (b) Picture of brecciated quartz veins containing silicified clasts. (c) Picture of the fault gouges with heterogeneous silicified clasts in the siliceous matrix. (d) Stereographic projection of bedding and faults orientation. See [Table 1](#) for brittle structure nomenclature.

## 4.1 Lithologies

### 4.1.1 Basement unit

The basement unit (B.U.) has been studied in detail at four sites from west to east: Anse aux Moines, Cayola Bay, Mine des Sardes, and Anse de Saint-Nicolas ([Fig. 2a](#)). Each site has a similar pattern corresponding to a tidal rocky shelf of several tens of meters wide separated from a 10 to 15 meters high coastal cliff by a more or less-developed beach, such as the cliff of the Anse aux Moines ([Fig. 4](#)). In each site, the basement unit occupies the tidal rocky shelf, and the unconformity separating the basement unit and the sedimentary cover can be observed along the coastal cliff in many places. Horizontal and panoramic orthoimages obtained by UAV ([Figs. 5a, 6c, and 8b](#) and in [Supplementary material](#)) provide practical support for G.I.S. tectonic structure mapping and field observation localization ([Figs. 5, 6, and 8](#)).

In the B.U., the gneissic foliation is synchronous with metamorphism ([Goujou \*et al.\*, 1994](#)) and magmatic intrusion ([Cagnard \*et al.\*, 2004](#)). The foliation strikes between N90° and N110° and plunges to the N with an angle between 40° and 60° at the Anse aux Moines ([Figs. 2a and 4](#)), Cayola Bay ([Fig. 5](#)), the Mine des Sardes ([Fig. 6](#)) and turns to N160–50°E at the

Anse de Saint-Nicolas ([Fig. 8](#)). In Cayola Bay, dikes are more or less transposed into the foliation ([Fig. 5a-b](#)).

### 4.1.2. Sedimentary units

We divided the Aquitaine Basin series into five sedimentary units called SU1, SU2, SU3, SU4, and SU5 ([Fig. 2b](#)) based on the sediment's age and lithologies and, thus, different mechanical behavior. The shallow dip (10°) of the bedding to the N or the S defines several large open folds offering good outcrop conditions on the plateau in each unit ([Fig. 2a](#)).

SU1 and SU2 have been dated from the Hettangian age on paleontological contents ([Bouton, 2004](#); [Goujou \*et al.\*, 1994](#); [Granier \*et al.\*, 2015](#)). They can be observed along the coastal cliffs of each site and on the part of the tidal rocky shelf in the Anse aux Moines, Cayola Bay, the Mine des Sardes, and the Anse de Saint Nicolas ([Figs. 4, 5, 6, and 8](#)). SU1 lies directly on the B.U. ([Figs. 4a, 5d-e, 6a-b, and 8a](#)). It consists of a 1 to 4 m thick grey clay-rich unit intercalated with layers of yellow dolomitic limestones ([Figs. 4a, 5d-e, and 6b](#)) except at the Anse de Saint-Nicolas area where it is replaced by a 20 cm thick conglomerate bed ([Fig. 8a](#); [Goujou \*et al.\*, 1994](#)).

**Table 1.** Fracture populations with their properties.

Population	Strike-Structure type	Unit affected	Figures	Unconformity	Mineral deposit (barite, pyrite, quartz, calcite)	Relative chronology
FP-1	N-S-normal fault -dike	BU	5,6,8	sealed by	∅	associated with dike
FP-2	NE-SW-sinistral fault	BU	5,6	sealed by	∅	syn FP-3
FP-2 (reactivated)	NE-SW-joint	BU to SU3	8	sealed by	Pyrite(±oxidized)	syn FP-4
FP-3	NNW-SSE dextral faults	BU	6	sealed by	∅	syn FP-2
FP-3 (reactivated)	NNW-SSE normal faults	BU to SU3	6,8	cutting	silification	syn FP-4
FP-4	WNW-ESE normal fault and veins	BU to SU5	4,5,6,7,8,9	cutting	Filled+silicification	abuting on FP-2 and FP-3
FP-5	WNW-ESE calcite vein	SU2	7	unknown	Calcite only	cutting FP-4 veins
JP-1	NE-SW joints	SU5	9	unknown	∅	syn JP-2, abuting on FP-4
JP-2	NNE-SSW joints	SU5	9	unknown	∅	syn JP-1, abuting on FP-4

The SU2 consists of a layer of dolomitic limestones 5 to 10 m thick with bed thickness ranging from 5 to 30 cm (Figs. 4a, 5d-e, and 6b). In this unit, karsts are abundant in some places, especially at the Mine des Sardes and the Anse de Saint-Nicolas, filled with barite and quartz (Fig. 6g-h). Karst shapes are mostly lenticular (Fig. 6g), parallel to the bedding with elongated WNW-ESE-tubular shapes. Silicification of SU2 limestones is very common in the Anse aux Moines, the Mine des Sardes, and the Anse de Saint-Nicolas (Figs. 4a, 5d-e, 6a, and 8a). In Cayola Bay (Fig. 5d-e), silicification only develops around faults crosscutting the BU/SU1 unconformity.

The SU3 is dated to the Plienbachian (Fauré and Bohain, 2017). The hardground at the top of SU2, the pebbles layer at the base of SU3, and the absence of Early Sinemurian fauna have been interpreted as evidence of emersion of the area between the Late Hettangian and Early Sinemurian (Fauré and Bohain, 2017). SU3 is visible on the coastal cliffs of the Mine des Sardes and the Payré estuary (Figs. 7a and 10c) and has been mapped on the tidal rocky shelf of the Anse de Saint-Nicolas (Fig. 8b). It consists of limestones with abundant Pecten and Belemnite fossils alternating with a shale-rich layer. Similarly to SU2, SU3 is silicified in places such as the Mine des Sardes.

The SU4 has been dated from the Toarcian to the Aalenian using paleontological contents (See reference in Goujou *et al.*, 1994). It is observed at the Anse de Saint-Nicolas coastal cliff (Fig. 8b) and, depending on the amount of sand and the tide, at the foot of the beach between the Anse de Saint-Nicolas and the Four à Chaux (Fig. 9a). It consists of a 20 m thick succession of blue shale and rare limestones that forms an impermeable layer on the scale of the northern Aquitaine Basin (Cathelineau *et al.*, 2012).

Based on paleontological contents, the SU5 has been dated from the Bajocian to the Callovian (Goujou *et al.*, 1994, and references therein). It outcrops at Four à Chaux and extends several kilometers to the east. It is a 100 m thick unit. It comprises white limestone beds 10 to 50 cm thick alternating with centimetric marl layers (Fig. 9d).

## 4.2 Brittle structure of the Vendée coastal domain

In the field, we observed fractures with sometimes mineral filling (veins) and faults with offset up to 10m from the B.U. to SU5. Slickensides are preserved in SU2 and SU5, giving the offset's orientation, but alteration (argillization and silicification) has erased them in B.U., making this measurement impossible. We estimate movement mainly by considering remarkable markers offsets such as dike, unconformity, lithological contacts, quartz lenses, and sedimentary beds.

### 4.2.1. Anse aux Moines outcrop

The westernmost outcrop is located at the Anse aux Moines (Figs. 2a and 4). It consists of a 150 m-long coastal cliff-oriented NNW-SSE. Here, the tidal rocky shelf is rarely visible at low tide, and a thick pebble beach limits observation of the cliff (Fig. 4). The outcrop consists of SU1 and SU2 rocks bounded north and south by the migmatitic gneisses forming the B.U. To the north, the B.U. is covered by SU1 and SU2 (Fig. 4a). The contact between the B.U. and the SU1 and SU2 bedding are parallel and inclined together to the south, suggesting that the unconformity outcrops here (Fig. 4a-d). The contact between B.U. and SU1 is steeper to the south and underlined by an N116–69°NNE normal fault plane (Fig. 4a). The fault zone is underlined by a 4 m thick fault gouge zone and strongly deformed SU1 beds (Fig. 4a-c). Silicification is well-developed, especially within the SU2 and the fault gouge breccias. Quartz also fills a 50 cm thick vein striking parallel to the fault (Fig. 4b). The structural pattern is consistent with a half-graben structure bounded by a north-dipping fault and tilted toward the south.

### 4.2.2. Cayola Bay outcrop

Cayola Bay is located at the estuary of the Combe River (Fig. 2a). It is a triangular-shaped bay bounded by two 500-m-long coastal cliffs. The one situated west is striking NNE-SSW, and the other, NW-SE. B.U.'s tidal rocky shelf is present



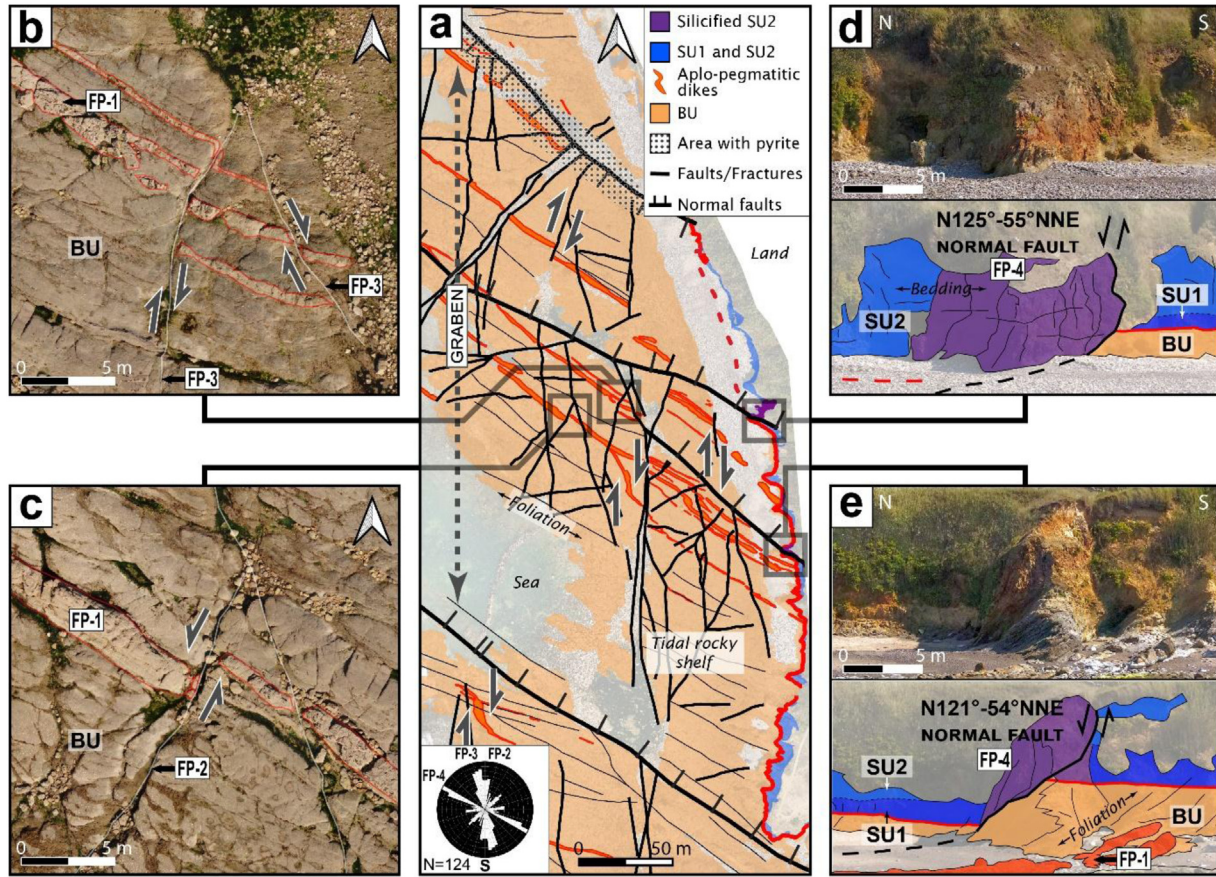


**Fig. 5.** Cayola Bay outcrop. (a) Interpreted UAV orthoimage of the S.E. side of the NW-SE oriented Cayola bay graben with fault motions reported and weighted rose diagram. (b) Orthoimage extract showing dextral ductile-brittle deformation of the aplo-pegmatitic dike (underlined in red) by NNW-SSE to N-S faults on the rocky shelf. (c) UAV Orthoimage extracts showing a sinistral deformation of the dike by NNE-SSW faults. (d) and (e) coastal cliff picture and interpretation of the normal faults shifting the unconformity and associated silicification of the cover. See [Table 1](#) for brittle structure nomenclature.

primarily on either side of the bay, and rocks from the SU1 and SU2 are visible on the coastal cliff. We focused here on the eastern part of the bay, where the unconformity is more visible.

On Cayola Bay ([Fig. 5](#)), we measured three populations of oriented brittle structure: N160° to N-S, N30° to N50° and N110° to N130° respectively. The N110–130° fault population is the only one to displace the unconformity suggesting an activity post-dating the Hettangian ([Fig. 5d-e](#)). In contrast, faults oriented N160° to N-S and N30° to N50° are sealed by the unconformity, suggesting a pre-Hettangian activity ([Fig. 5d-e](#)).

Aplo-pegmatitic dikes injected into the B.U. allow us to estimate the apparent offset of the faults. N160° to N-S striking faults cut aplo-pegmatitic dikes with an apparent dextral offset ([Fig. 5a-b](#)). At several locations, their orientation continuously evolves from an NW-SE to an N-S strike with the same sense of shearing ([Fig. 5a-b](#)). This suggests that N160° to N-S oriented faults may have been active during the dike emplacement. N30° to N50° striking faults cut aplo-pegmatitic dikes with apparent sinistral offsets ([Fig. 5c](#)). Together, the N160° to N-S striking faults and the N30° to N50° striking faults may have been active simultaneously as conjugated faults.

Three major N110° to N130° striking faults were mapped on the tidal flat and the coastal cliff ([Fig. 5a-e](#)). No dike offsets were observed because these faults strike in the same direction as metamorphic foliation and aplo-pegmatitic dikes ([Fig. 5a-e](#)). However, in the coastal cliff, the unconformity is crosscut by these three faults with normal motion ([Fig. 5d-e](#)). Around N110° to N130° striking normal faults, SU2 limestones are locally silicified over a width of 1 to 3 m ([Fig. 5d-e](#)). In the B.U., the northernmost fault is filled with pyrite mixed with host rocks ([Fig. 5a](#)). The opposite dipping of N110° to N130° striking normal faults toward Cayola Bay delineates a graben where the unconformity is lowered by 5 to 10 m ([Fig. 5a](#)).

#### 4.2.3. Mine des Sardis outcrop

The Mine des Sardis is located between Cayola Bay and Bourgenay ([Fig. 2a](#)). It is a large area where B.U. is observed on the tidal rocky shelf, and SU1 and SU2 are primarily visible on the coastal cliff ([Fig. 2a](#)). Unfortunately, the unconformity is rarely visible as it is covered by beach pebble deposits.

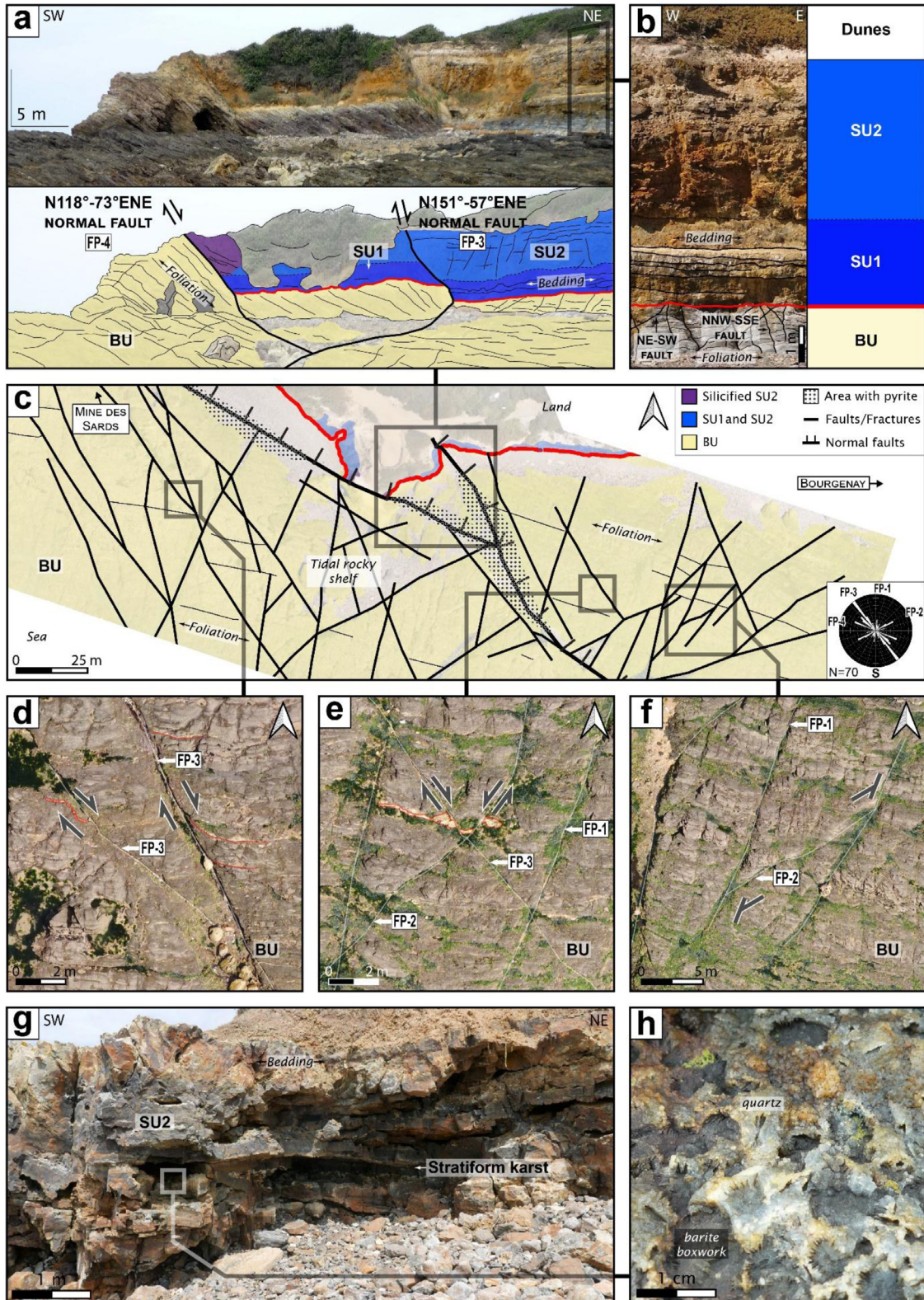


**Fig. 6.** Mine des Sardis outcrops. (a) Picture of two normal faults spreading in the cliff, shifting the unconformity. (b) Picture of the cliff showing B.U. to SU2 and the non-spreading of NE-SW and NNW-SSE faults from B.U. above the unconformity. (c) Interpreted orthoimage of the rocky shelf with weighted rose diagram. (d) Orthoimage extract showing a dextral brittle deformation of the foliation (underlined in red) by WNW-ESE faults in B.U. (e) Orthoimage extract showing conjugate faults shifting a syn-foliation quartz dike (underlined in red). (f) Orthoimage extract showing a NE-SW fracture abutting on NNE-SSW faults. (g) and (h) pictures of stratiform karsts from the Mine des Sardis in the silicified SU2 with barite and quartz mineralization on the karst walls. See Table 1 for brittle structure nomenclature.

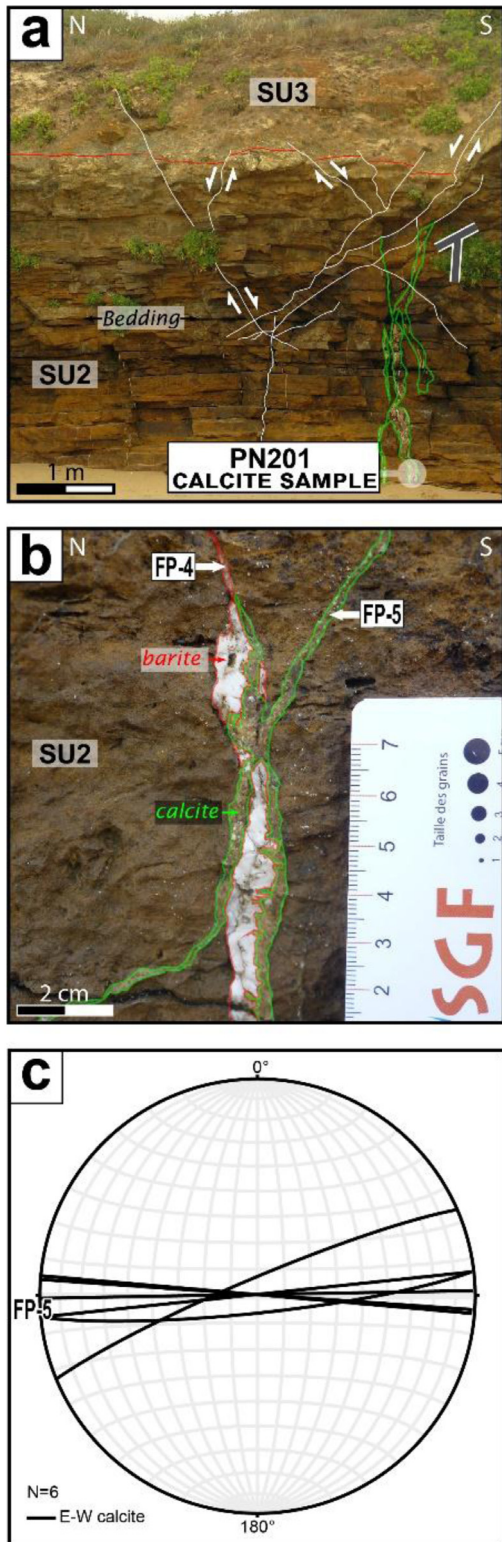


**Fig. 7.** Payré Estuary outcrop. (a) Picture of the cliff showing the erosive surface between SU2 and SU3, and barite-calcite-filled fractures that abut on normal faults. (b) Close up in SU2 of “teeth” shape calcite in vein crosscutting a barite-vein (underlined in red). (c) Stereographic projection of structure measured (bold black lines correspond to E-W “teeth” shape calcite-veins). See Table 1 for brittle structure nomenclature.

The area’s western boundary consists of an N160° and vertical fault that cuts SU1 to SU3 and uplifts B.U. (Fig. 2a). Here, we estimate a vertical offset of 5 to 10 m high because the uppermost SU3 is in direct contact with B.U. The latter changes from kyanite micaschists to the east of the fault to kyanite-sillimanite gneisses to the west. Such a change suggests that either the vertical offset was underestimated or the fault developed on a pre-existing contact (Fig. 2a). To the east, the B.U. is progressively covered by sedimentary units and disappears on the east side of Bourgenay (Fig. 2a).

The orthoimage in Figure 6 is located around 500 m east of the Mine des Sardes (Fig. 2a) in an area where the unconformity is well exposed. Here on the tidal rock platform, we measured four populations of brittle structure according to their orientations: N-S, N40° to N60°, N110° to N130°, and N140° to N160°. On the coastal cliff, the main N110° to N130° striking fault (oriented N118°–73°ENE) cuts the unconformity, SU1 and SU2 (Fig. 6a-c) and therefore is active after the Hettangian. The activity of the N-S, N40 to N60 striking fault population predates the Hettangian as they are always sealed by the unconformity (Fig. 6b). The relationship between the N140° to N160° striking fault population and the sedimentary units (SU1 and SU2) is more controversial as most of the structures are sealed by the unconformity (Fig. 6b) except one fault (oriented N151°–57°ENE) that produces a 1 m offset (Fig. 6a-c).

The N-S faults are vertical or dip mainly to the east, and their movement is not constrained because of bad outcropping conditions (Fig. 6b-c). The N40° to N60° and N140° to N160° striking faults are left and right lateral strike-slip faults, as evidenced by the offset of the foliation and the quartz lenses (Fig. 6d-e). They form an “X” shaped intersection compatible with conjugated fault abutting on N-S faults (Fig. 6f). All these faults are sealed by the unconformity (Fig. 6b) except one fault oriented N140° to N160° that cuts the unconformity (Fig. 6a-c).

A main N110° to N130° striking fault can be followed at the foot of the pebble beach and on both sides of a little cape (Fig. 6a-c). Here, the 3-4-m high unconformity offset is consistent with a normal motion. In SU2, pervasive silicification follows the normal fault planes and, in some places, propagates horizontally into the inter-stratum spaces. To the east, this normal fault abuts the N140° to N160° normal fault that cuts the unconformity (Fig. 6a-c). Despite their different orientations, both of these normal faults are filled by pyrite (Fig. 6c). This N140° to N160° normal fault could have been reactivated at the same time as the N110° to N130° faults.

#### 4.2.4. Payré Estuary outcrop

The Payré Estuary is a 250 m-long cliff area where SU2 and SU3 outcrop (Figs. 2a and 7a).

SU2 and SU3 are cut by a network of minor normal faults showing an offset of up to 10 cm (Fig. 7a). Besides, vertical E-W fractures (Fig. 7c) are filled with barite and calcite abutting on the previous normal fault network (Fig. 7a). At the fracture scale, the calcite veins crosscut the barite vein (Fig. 7b). A last calcite mineralization stage is locally observed in the coating (concretionary habit) both in the fractures and the interbeds.

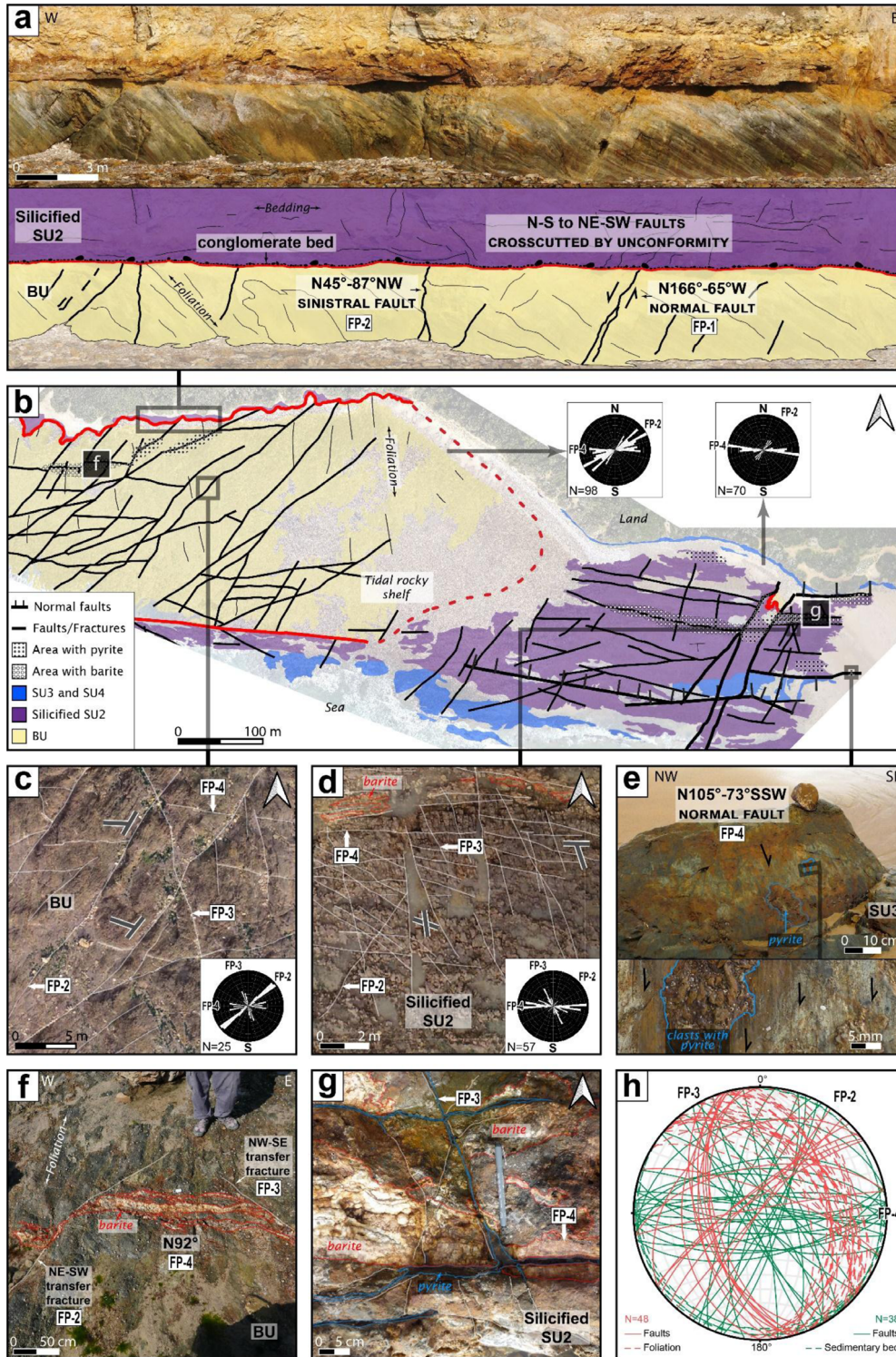


**Fig. 8.** Anse de Saint-Nicolas outcrop. (a) Picture of the cliff on the west side of the Anse de Saint-Nicolas showing B.U. covered by SU2 and NW-SE sinistral faults and N-S normal fault hosted in the B.U. crosscut by the unconformity. (b) Interpreted orthoimage of the rocky shelf made of B.U. to SU4 with weighted rose diagrams. SU2 hosts WNW-ESE normal faults and NE-SW brecciated structure with pyrite. (c) Orthoimage extract showing WNW-ESE fractures abutting on NE-SW faults in B.U. with weighted rose diagrams. (d) Orthoimage extract showing N-S fractures abutting on and crosscutting WNW-ESE fractures locally filled by barite with weighted rose diagrams. (e) Picture of a fault mirror of a WNW-ESE normal fault with a pyrite patch and a zoom with vertical slickenside. (f) View of a barite vein in B.U. (g) Picture of barite filling E-W fractures in veins and geodes crosscut by E-W and NNW-SSE pyrite vein. (h) Stereographic projection of structure measured in B.U. (red lines) and SU2 (green lines). See Table 1 for brittle structure nomenclature.

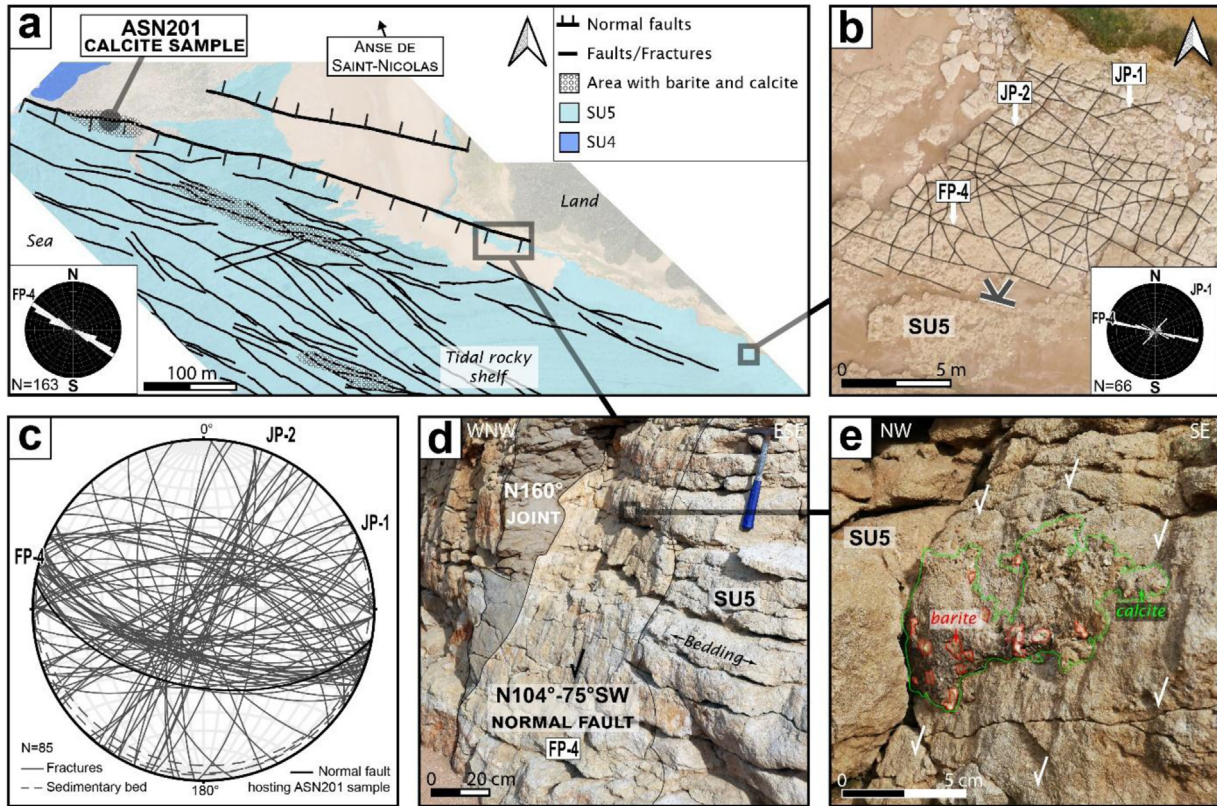


**Fig. 9.** Four à Chaux outcrop. (a) Interpreted UAV orthoimage of the rocky shelf and weighted rose diagrams of the digitized faults and fractures. (b) Orthoimage extract showing NNW-SSE and NW-SE fractures both abutting on and crosscutting WNW-ESE fractures with weighted rose diagrams of the digitized fractures. (c) Stereographic projection of structure measured in SU5. (d) and (e) Pictures of the fault mirror of the normal fault hosting ASN201 sample showing barite (underlined in red) and calcite (underlined in green) associated with vertical slickenside. See [Table 1](#) for brittle structure nomenclature.

#### 4.2.5. Anse de Saint-Nicolas outcrop

The Anse de Saint-Nicolas is a large area where unconformity can be followed in the middle of the coastal cliff over a distance of 1.5 km ([Fig. 2a](#)). The mapped zone is located at the eastern boundary of the cliff where B.U. and SU2 to SU3 are observed on the tidal rocky shelf ([Fig. 8b](#)). In the following section, we described the structure within the B.U. and those in SU2 to SU3.

The B.U. outcrops on the western half of the map ([Fig. 8a-b](#)). The foliation of the B.U. is striking N135° to N0° and dips to the east. In the field, we measured two populations of faults: 1) a west-dipping, N160°-trending normal faults spaced 20 to 50 cm apart ([Fig. 8a](#)) and 2) N40° to N60°-trending vertical left-lateral strike-slip faults ([Fig. 8h](#)). Both populations are sealed by the unconformity ([Fig. 8a](#)) and predate the Hettangian. The N40° to N60° striking faults are less numerous and locally form deformation corridors where pyrite is abundant ([Fig. 8b](#)). The orthoimage reveals N90° to N110° striking faults parallel to the coastal cliff ([Fig. 8a-b](#)). They abut on N40° to N60° striking faults ([Fig. 8c](#)) and are locally filled with barite, pyrite, and quartz ([Fig. 8f](#)).

SU2 and SU3 outcrop on the eastern half of the map ([Fig. 8a-b](#)) in this area, the structural pattern is dominated mainly by N90° to N110° striking fractures consisting of faults, veins, and joints ([Fig. 8b](#)). The fault offsets are consistent with

a normal motion and coherent with a vertical slickenside on a fault plane ([Fig. 8e](#)). The N90° to N110° striking veins are filled mainly with barite, pyrite ([Fig. 8g](#)), and occasionally with quartz ([Fig. 2a](#)). Geodic barites are abundant in the E-W corridors ([Fig. 8b-g](#)). The unconformity is visible on the coastal cliff and in most distal parts of the rocky tidal shelf, where a 500 m-long outcrop of silicified SU2 is preserved ([Fig. 8b](#)). As at the Anse aux Moines, Cayola Bay, and the Mine des Sardes ([Figs. 4, 5, and 5](#)), silicification of SU2 develops over a few meters around N90° to N110° striking normal faults, potentially increasing SU2's resistance to erosion.

In SU2 and SU3, two further populations of smaller fractures striking from N30° to N50° and N150° to N170° ([Fig. 8b-h](#)). As no offsets of the sedimentary beddings are observed here, this suggests a type I rupture mode (*i.e.*, joints). These smaller fractures are locally filled with pyrite, while barite is always absent ([Fig. 8g](#)). No structure striking between N150° and N170° are visible at the map scale, but they do appear at high resolution ([Fig. 8d-g](#)). In many locations, abutment relationships indicate that N150° and N170° striking joints post-dates N90° to N110° striking fractures ([Fig. 8d-g](#)). The N30° to N50° striking fracture population is well expressed at the map scale, where it forms a linear corridor with abundant pyrite embedding angular clasts but with no visible motion ([Fig. 8b](#)). However, the geometric relationship

between this corridor and the N90° to N110° striking faults remains unclear. At high resolution, the “X” shape geometry of the N150° to N170° striking joints and the N30° to N50° striking joints (Fig. 8d-g) suggests that they act as conjugated joints.

#### 4.2.6. Four à Chaux outcrop

Four à Chaux is located east of Anse de Saint-Nicolas (Fig. 2a), where SU4 and especially SU5 are observed on the tidal rocky shelf and the coastal cliff (Fig. 9a-d). A major fault described by Ters and Gabilly (1986) draws SU5 down to the level of SU4 in the north-western part of the mapped area.

Field measurements (Fig. 9c) and the ortho-image in Figure 9a-b highlight three fracture populations oriented respectively: N100° to N120°, N40° to N60° and N160° to N-S°. Fractures oriented N100° to N120° are the longest structure with local barite and calcite fillings (Fig. 9a-e). On the coastal cliff, the slickensides on a fault plane oriented N104°–75°SW are compatible with a normal motion (Fig. 9e).

The N40° to N60° and N160° to N-S° fractures are the shortest; they are visible only at a high resolution between the beach and the coastal cliff (Fig. 9b). These two fracture populations are abutting and thus post-dated on the N100° to N120° striking fractures (Fig. 9b). The geometrical relationship between the N40° to N60° and the N160° to N-S° striking fractures are an “X” shape intersection suggesting that these two populations are coeval (Fig. 9b). No offsets of the sedimentary bedding are observed here, suggesting a type I opening mode (*i.e.*, joints). No mineralization fills these joints (Fig. 9d).

#### 4.3 Calcite U-Pb geochronology

The three samples for U-Pb dating are from calcite veins sampled at Four à Chaux (ASN201 sample; Fig. 9a) and at the Payré Estuary (PN201 and PP5 samples; Fig. 7a).

ASN201 has been sampled on the tidal rocky shelf of Four à Chaux composed of SU5 strata (Fig. 10a), where calcite forms 10 cm thick veins with dilational vein textures (Fig. 10b; Roberts and Holdsworth, 2022). Its orientation is N100°–52°S (Fig. 10b), and at the map scale, it is the continuation of the major normal fault N104°–75°SW (Figs. 9a and 10a). On the cliffs, slickensides from the fault plane indicate a normal sense of shearing and the occurrence of rosette-shaped barite with calcite on the fault plane surface (Fig. 9d-e). The mineral deposition is synchronous with the fault activity (Roberts and Holdsworth, 2022). ASN201 sample consists of yellowish subtransparent rhombohedral calcite crystals 0.5 to 1 cm wide. At a small scale, the calcite vein hosts crackle-breccia of SU5 embedded by the same blocky calcite crystals (Fig. 10c). This observation demonstrates the synchronous precipitation of calcite with the faulting that affects SU5. The lower intercept on the Tera-Wasserburg Concordia diagram yields a date of  $144.1 \pm 26.2 / 26.4$  Ma ( $n=20$ , MSWD=0.68; Fig. 10g).

Samples PN201 and PP5 come from the Payré Estuary coastal cliff (Figs. 2a and 7). PN201 and PP5 are oriented N86°–84°S and N95°–88°S respectively (Fig. 5d). These veins are hosted in SU2, and by place, the veins crosscut barite

veins, like the sample PN201 (Figs. 7b and 10d). This shows that two fracturing with N-S opening occurred at the Payré Estuary, the first with fractures filled by barite and the second with calcite. In detail, the calcite consists of cloudy yellowish-white rhombohedral crystals 1 to 3 cm wide. At a small scale, in a smaller sample than PN201 from the Payré Estuary cliff, a barite vein is crosscut by a calcite vein constituted of blocky crystals (Fig. 10f). Another calcite veinlet filled a fracture crosscutting the same barite vein (Fig. 10f). The morphology of the calcite veins could suggest a single phase opening during crack-seal, and so, possible synchronicity of calcite filling with fracturing (Roberts and Holdsworth, 2022). The lower intercept on the Tera-Wasserburg Concordia diagram yield dates of  $72.5 \pm 11.5 / 11.6$  Ma ( $n=20$ , MSWD=0.45) and  $79.7 \pm 22.3 / 22.4$  Ma ( $n=20$ , MSWD=0.85), for PP5 and PN201 calcites respectively (Fig. 10 h-i).

## 5 Discussion

### 5.1 Chronology of brittle structure

From site to site, we sorted the joints and faults in the Vendée coastal domain according to their 1) orientations, 2) relationships to the Aquitaine Basin unconformity, and 3) mineral fill (Tab. 1). We obtained five populations of faults and two populations of joints (referred to after that as FP-1 to FP-5 and JP-1 and JP-2).

The FP-1 fracture family consists of N-S striking normal faults crossing only B.U. (Figs. 5, 6, and 8). They are locally associated with the emplacement of aplo-pegmatitic dikes (Fig. 5), suggesting that they were active at the end of the Variscan ductile deformation dated from Late Carboniferous by Turrillot *et al.* (2011) and Augier *et al.* (2015).

The FP-2 fracture family consists of NE-SW striking sinistral faults that displace beddings relics in B.U. micaschists and magmatic dikes with an apparent horizontal offset of up to 5 m (Figs. 6 and 8). The FP-2 is sealed by the Aquitaine Basin unconformity everywhere in the B.U., indicating that they formed before the Hettangian. Because no magmatic dike follows the fault plane of FP-2, we propose that FP-2 post-dates FP-1. In the Anse de Saint-Nicolas area, NE-SW joints of the same orientation crosscut SU2 and SU3. No strike-slip motions were observed there. As these joints are not observed in SU4 and SU5, FP-2 is potentially reactivated between Pliensbachian and Toarcian times. However, as FP-2 from B. U., SU2, and SU3 are filled with pyrite, the reactivation can also occur during the mineral deposition (referred to as FP-2 reactivated in Tab. 1). In this case, the absence of the NE-SW joint in SU4 and SU5 may be explained by the rheologic barrier of the SU4 marls, as in the case of mineral deposits.

The FP-3 fracture family consists of NW-SE striking dextral faults that cut and shift bedding relics in B.U. micaschists and aplo-pegmatitic dikes (Fig. 6). The relationship between FP-3 and the Aquitaine Basin unconformity is ambiguous: on the one hand, FP-3 is sealed by the unconformity in most cases, indicating that it formed before the Hettangian. At B.U., it abuts FP-1 and thus is posterior to FP-1 (Fig. 6), and the intersecting relationship between FP-3 and FP-2 suggests that they formed simultaneously. On the other hand, two major faults from FP-3 crosscut the unconformity with a normal motion, and SU2 and SU3 at

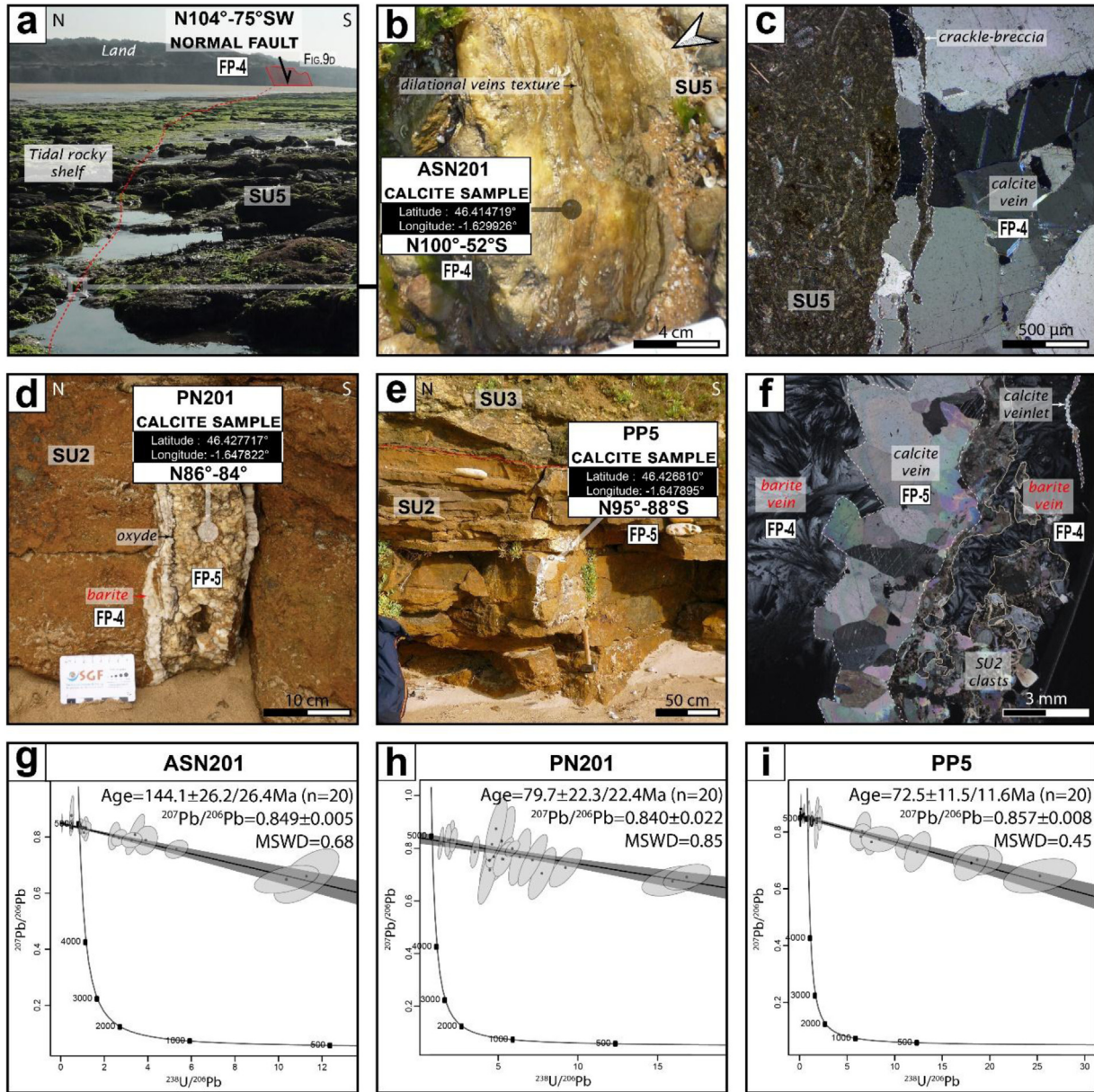


**Fig. 10.** Calcite samples dating. (a) Field picture of the sampling area of ASN201 showing the disposition with the fault plane in [Figure 9d](#). (b) Field picture of ASN201 sample with a texture similar to dilational veins ([Roberts and Holdsworth, 2022](#)). (c) A small-scale petrographic picture under polarized light of ASN201 sample. SU5-breccias along the wall of the calcite vein are embedded by the same calcite crystals (same extinction orientations), attesting that calcite precipitated during fracturing. (d) and (e) field pictures of PN201 and PP5, respectively. PN201 calcite vein reopened barite vein. (f) A small-scale petrographic picture under polarized light of a sample from the Payré Estuary outcrop, similar to PN201. The calcite vein is crosscutting barite vein along the interface with an SU2 clasts. Another sub-parallel calcite veinlet crosscuts the barite vein in the upper left corner. (g), (h) and (i) Tera-Wasserburg Concordia diagrams of dated calcite samples, uncertainties are given without and with systematic uncertainties. See [Table 1](#) for brittle structure nomenclature.

the contact of these two faults are silicified (Figs. 2 and 6). These mean the reactivation of FP-3 per place (referred to as FP-3 reactivated in Tab. 1).

The FP-4 fracture family consists of WNW-ESE striking normal faults that affect both B.U. and SU1 to SU5 (Figs. 4–9) and with the Aquitaine Basin unconformity (Figs 4–6). The FP-4 structure family forms horsts and grabens visible at map scale (Figs. 2, 4, and 5). FP-4 abuts FP-2 and FP-3, suggesting that these latter predate FP-4 although they crosscut the unconformity (Figs. 2 and 6). We observed barite, pyrite, quartz, and calcite-filled veins and fault planes in the SU1 to SU5 as previously described by Cathelineau *et al.* (2012) and Strzeczynski *et al.* (2020) but also in the B.U. (Fig. 8). We also provide field evidence of focused silicification of SU2 and SU3 immediately around FP-4 faults that crosscut the unconformity (Fig. 4). Given this evidence, we propose that the fluid flow related to mineral deposition and silicification is contemporaneous with normal faulting. Calcite from sample ASN201 which fills an FP-4 affecting SU5 yields a U-Pb date of  $144.1 \pm 26.2$  Ma (Fig. 10). In the same fault plane, calcite is associated with barite (Fig. 9a–e). This date overlaps the 155 to 145 Ma interval proposed in the northern Aquitaine Basin ( $^{40}\text{Ar}/^{39}\text{Ar}$  and K-Ar dating on adularia and clays by Cathelineau *et al.*, 2012). It reflects the timing of mineral deposition and WNW-ESE striking normal faulting (Fig. 9).

The FP-4 fracture family consists of WNW-ESE striking calcite veins that affect SU2 in the Payré Estuary (Fig. 7). The FP-5 veins crosscut the FP-4 barite veins (Fig. 7) and abut on FP-4 normal fault. Calcite from samples PP5 and PN201 that fills FP-5 veins yield a U-Pb date of  $72.5 \pm 11.5$  Ma and  $79.7 \pm 22.3$  Ma, respectively (Fig. 10). These ages are significantly younger than the 170 to 118 Ma range proposed for FP-4 and agree with the relative chronology (Fig. 7).

The JP-1 and JP-2 joint families, oriented NE-SW and NNW-SSE, respectively (Fig. 9), only develop in SU5 (Fig. 9). Both are abutting on, and thus they post-date FP4. The absence of barite, pyrite, quartz, and calcite filling the joints confirms that JP-1 and JP-2 post-date mineral deposition (Fig. 9). In the absence of observed relationships with FP-5, the relative timing remains unconstrained.

## 5.2 Late-Variscan tectonic evolution

Three populations of faults (FP-1, FP-2, and FP-3) sealed by unconformity take place before the Hettangian (Fig. 11). The orientation and movements of FP-1 are consistent with E-W extension post-dating HT-LP Variscan metamorphism (Cagnard *et al.*, 2004; Goujou *et al.*, 1994; Iglésias and Brun, 1976). A population of similar faults observed in the west Armorican Massif has been dated between 302 and 298 Ma (Turrillot *et al.*, 2011). The geometric relationship between FP-3 and FP-2 suggests synchronous and conjugate slip faults compatible with  $\sigma_1$  and  $\sigma_3$ , oriented N-S and E-W, respectively (Fig. 6) and consistent with the dextral movement of the South Armorican shear zone (Fig. 2) that ended circa 300 Ma (Augier *et al.*, 2015). Considering this, we propose that brittle faults of the Vendée coastal domain sealed by the Aquitaine Basin unconformity occur during the Late Carboniferous (Fig. 11). No further deformation is recognized until the deposition of SU1.

## 5.3 Late-Jurassic Early Cretaceous extension and fluid event

The FP-4 structure are compatible with a subhorizontal  $\sigma_3$  oriented N-S, as Strzeczynski *et al.* (2020) proposed. Throughout the study area, tectonic activity is synchronous with fluid transfer and mineral deposition (Cathelineau *et al.*, 2012; Strzeczynski *et al.*, 2020) (Figs. 2 and 11). The close relationship between high-temperature mineral deposition ( $> 250^\circ\text{C}$ ), silicification, and the rooting of FP-4 normal faults in the B.U. suggests that some of the fluids involved are crustal in origin and ascend from several kilometers depth (Cathelineau *et al.*, 2012). Our new age on FP-4 calcite constrains the chronology of N-S extension in the Vendée coastal domain at the Jurassic-Cretaceous transition (Fig. 10 and 11). This age is consistent with previous dating of adularia and clay minerals (Cathelineau *et al.*, 2012), meaning the dated minerals precipitated simultaneously. This event predates the main extensional phase of Aquitaine Basin rifting and oceanic spreading in the Bay of Biscay (Fig. 1; Tugend *et al.*, 2014, 2015) and is related to the earliest extensive deformation (Asti *et al.*, 2022).

The barite, pyrite, and quartz deposits that fill several faults FP-2 and FP-3 (Fig. 8) show that during the Jurassic-Cretaceous transition, at the Jurassic-Cretaceous transition, fluids flow along both newly formed (FP-4) and reactivated (FP-2 and FP-3) structure. In addition, we document the tectonic reactivation of the inherited strike-slip fault FP-3 during the Jurassic-Cretaceous transition fluid event (Fig. 6). The involvement of the Late Variscan inherited structure during the rifting phase of the Aquitaine Basin has been proposed before based on seismic profiles (Ducoux *et al.*, 2021; Issautier *et al.*, 2020; Manatschal *et al.*, 2015) but never observed in the field. The Vendée coastal domain provides a unique opportunity to observe the association of newly formed and inherited faults during this rifting phase. This fault association agrees with the oblique rifting model for the Bay of Biscay proposed by Asti *et al.* (2022).

## 5.4 Pyrenean compression

A calcite-filled FP-5 fracture dated between 84 and 61Ma (Fig. 10) and joints JP-1 and JP-2 post-date the mineralization and extension of the Jurassic-Cretaceous transition. If calcite infilling is synchronous with FP-5, the latter forms with the onset of shortening along the Eurasian-Iberian plate boundary (Fig. 1). At this time, shortening is assumed to follow an NNE-SSW direction (Rocher *et al.*, 2000) parallel to the  $\sigma_3$  opening direction of the FP-5 stage veins (Figs. 7 and 11). In convergent domains, subhorizontal  $\sigma_3$  strike in the same direction as large-scale convergence has already been described before and during thrusting (Lacombe, 2010, 2012). When it precedes horizontal shortening, subhorizontal  $\sigma_3$  stress is related to extension into the peripheral foredeep bulge (Bradley and Kidd, 1991; Doglioni, 1995; Langhi *et al.*, 2011; Tavani *et al.*, 2015; Turcotte and Schubert, 2002). When subhorizontal  $\sigma_3$  stress coincides with shortening, it corresponds to limited extension at fold hinges (Cooper, 1992; Hancock, 1985).

During the Late Cretaceous (pre-Santonian), the extension observed in the Aquitaine Basin foreland is associated with



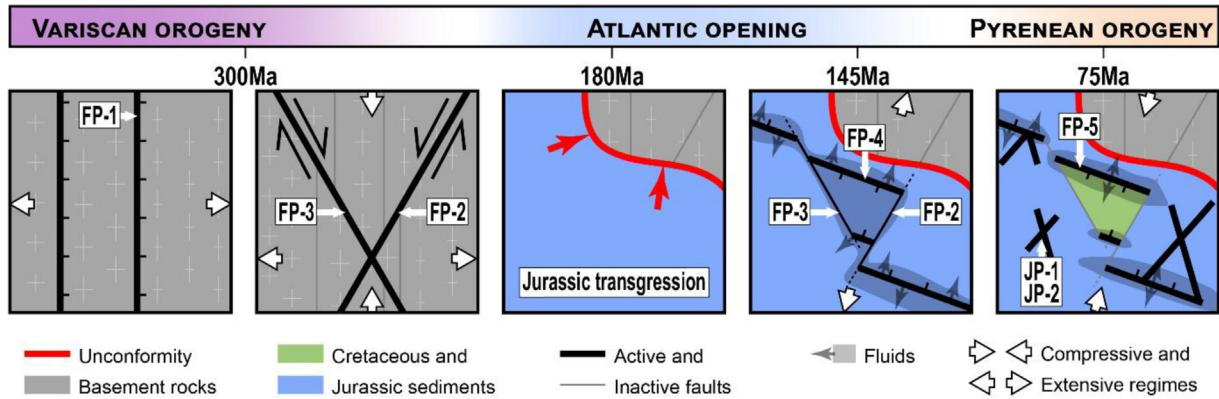


**Fig. 11.** Schematic diagrams of Vendée Coast brittle structure from the tectonics of the Late Variscan Orogeny (FP-1, FP-2, and FP-3), the Early Jurassic transgression covering the Variscan basement, the Atlantic Opening (FP-4 and partial reactivation of FP-2 and FP-3) and the Pyrenean Orogeny (FP-5, JP-1, JP-2, and fold). See Table 1 for brittle structure nomenclature.

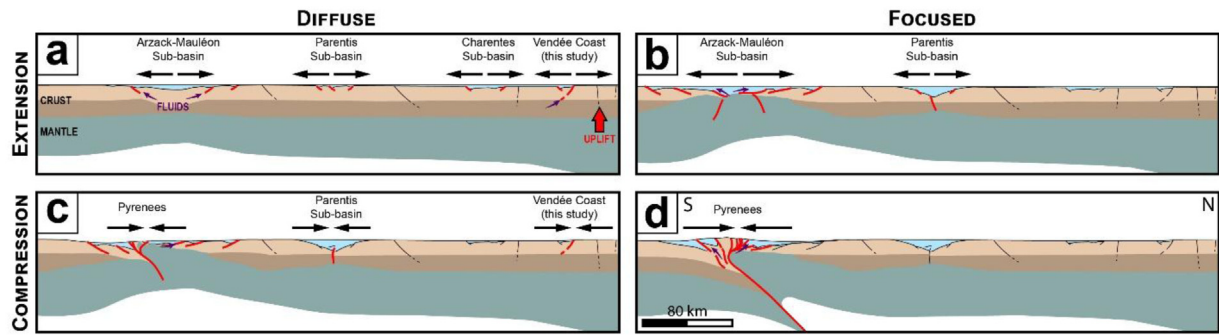


**Fig. 12.** Evolution of an N-S cross-section through the Aquitaine Basin showing the tectonic activity and where it distributes from (a) Late Jurassic – Early Cretaceous, (b) Early Cretaceous, (c) Late Cretaceous to (d) Paleogene.

mantle exhumation leading to high geothermal gradients (e.g., Angrand *et al.*, 2018; Clerc *et al.*, 2012; Issautier *et al.*, 2022; Lagabrielle and Bodinier, 2008; Lagabrielle *et al.*, 2010). This thermal influence does not affect the northern Aquitaine Basin. In the Vendée coastal domain, two joints (JP-1 and 2) and folds (Fig. 2) could be due to NNE-SSW compressive deformations (Fig. 11) after the extension of the Late Jurassic and Early Cretaceous. Thus, compressive tectonics related to the Campanian Iberia-Eurasia convergence (Issautier *et al.*, 2022; Mouthereau *et al.*, 2014; Roure *et al.*, 1989; Vergès *et al.*, 1995, 2002) is observed during the Late Cretaceous up to 400 km north of the Pyrenean belt.

### 5.5 Diffuse versus focused strains in the Aquitaine-Pyrenean domain

Our new constraints on the timing of the deformations affecting the North Aquitaine Platform provide insight into how diffused tectonics focused on limited areas during kinematic changes at plate boundaries.

The exhumation of the Armorican Massif and the French Massif Central began in the Late Jurassic and/or Early Cretaceous from the initiation of the opening of the Bay of Biscay (Figs. 1 and 12; Barbarand *et al.*, 2020; François *et al.*, 2020). Such uplift coincides with forming of new fault

networks (FP-4) on the North Aquitaine Platform, compatible with subhorizontal  $\sigma_3$  oriented N-S and the tectonic reactivation of inherited faults (FP-3). In the Paris Basin, this episode results in large-scale folding, forced regression, and unconformity deposition of Purbeck facies (Brigaud *et al.*, 2018). These observations provide good arguments for intra-plate deformation (e.g., Parizot *et al.*, 2022; Ziegler *et al.*, 1995).

Because it occurred 30 Ma before the main Aquitaine rifting event and is located 350 km north of the main rifts in the Parentis and the Arzack-Mauléon Basins, we proposed that extension in the Vendée coastal domain at the Jurassic to Cretaceous transition is an example of diffuse extension terrain preceding the focus of strain during rifting (Fig. 12; Asti *et al.*, 2022; Huerta and Harry, 2007; Seymour *et al.*, 2016; Szymanski *et al.*, 2016).

A network of calcite-filled conjugate joints and faults (FP-5) (Fig. 7), crosscutting the previous fractures (FP-4), are Late Cretaceous, *i.e.*, from the early stages of the Iberian-Eurasian convergence. At this time, no temperature drop occurred in the Armorican Massif and the French Massif Central (Barbarand *et al.*, 2020; François *et al.*, 2020), suggesting that shortening is not associated with significant uplift of the North Aquitaine Platform. As no relief is documented (Huyghe *et al.*, 2012), such compressive deformation cannot be related to wedge propagation. It is

more likely related to far-field intra-plate tectonics (Fig. 12; Gorczyk *et al.*, 2013) predating the formation of the Pyrenean relief and the Eocene propagation of the deformation in the North Aquitaine Platform (Brown *et al.*, 2021), the Paris basin (Blaise *et al.*, 2022) and the English Channel (Parrish *et al.*, 2018).

## 6 Conclusion

In this study, we applied field and UAV imagery methods in the Vendée remarkable outcrops to decipher the evolution of brittle tectonics of the north of the Aquitaine Basin during the opening of the Bay of Biscay and the Iberia-Eurasia convergence.

We showed that: (1) During the opening of the Bay of Biscay, newly formed normal faults associated with reactivated Late Variscan faults provide evidence of oblique rifting. (2) Compressive tectonics related to the Iberia-Eurasia convergence occurred during the Late Cretaceous 400 km north of the Pyrenean belt. (3) Both the extensional and compressive tectonics are related to diffuse intra-plate tectonics before the focus of deformation on continental rifts and the Bay of Biscay during the Early Cretaceous and on the Pyrenean- Cantabrian margin during the Cenozoic.

## Supplementary Material

**Electronic Material 1:** Operating conditions for dalcite U-Pb dating.

**Supplementary Figure 1:** AUG-B6 secondary RM results for the six analytical sessions in which we used GeOHeLiS platform

The Supplementary Material is available at <https://www.bsgf.fr/10.1051/bsgf/2023014/olm>.

**Acknowledgments.** The TELLUS-CESSUR and AO-OSUNA programs have funded the research presented in this article. The authors thank Thomas Blaise and Michael Jentzer for helpful and constructive manuscript reviews.

## References

- Anderson EM. 1951. The dynamics of faulting. *Trans Edinb Geol Soc* 8.3: 387–402.
- Angrand P, Ford M, Watts AB. 2018. Lateral variations in foreland flexure of a rifted continental margin: The Aquitaine Basin (SW France). *Tectonics* 37: 430–449.
- Asti R, Saspiturry N, Angrand P, 2022. The Mesozoic Iberia-Eurasia diffuse plate boundary: A wide domain of distributed transtensional deformation progressively focusing along the North Pyrenean Zone. *Earth-Sci Rev* 230: 104040.
- Augier R, Choulet F, Faure M, Turrillot P. 2015. A turning-point in the evolution of the Variscan orogen: the ca. 325 Ma regional partial-melting event of the coastal South Armorican domain (South Brittany and Vendée, France). *Bull Soc Geol Fr* 186: 63–91. <https://doi.org/10.2113/gssgfbull.186.2-3.63>
- Ballèvre M, Bosse V, Ducassou C, Pitra P. 2009. Palaeozoic history of the Armorican Massif: Models for the tectonic evolution of the suture zones. *Comptes Rendus Geosci, Mécanique de l'orogénie varisque: Une vision moderne de la recherche dans le domaine de l'orogénie* 341: 174–201. <https://doi.org/10.1016/j.crte.2008.11.009>
- Barbarand J, Préhaud P, Baudin F, Missenard Y, Matray JM, François T, *et al.* 2020. Where are the limits of Mesozoic intracontinental sedimentary basins of southern France? *Mar Pet Geol* 121: 104589. <https://doi.org/10.1016/j.marpetgeo.2020.104589>
- Barré G, Fillon C, Ducoux M, Mouthereau F, Gaucher EC, Calassou S, 2021. The North Pyrenean Frontal Thrust: structure, timing and late fluid circulation inferred from seismic and thermal-geochemical analyses of well data. *Bull Soc Geol Fr* 192: 52. <https://doi.org/10.1051/bsgf/2021046>
- Bergerat F. 1987. Stress fields in the European platform at the time of Africa-Eurasia collision. *Tectonics* 6: 99–132.
- Biteau J-J., Marrec AL, Vot ML, Masset J-M. 2006. The Aquitaine Basin. *Pet Geosci* 12: 247–273. <https://doi.org/10.1144/1354-079305-674>
- Blaise T, Khoudja SAA, Carpentier C, Brigaud B, Missenard Y, Mangenot X, *et al.* 2022. Far-field brittle deformation record in the eastern Paris Basin (France). *Geol Mag* 1–15. <https://doi.org/10.1017/S0016756822000772>
- Boiron M-C., Cathelineau M, Richard A. 2010. Fluid flows and metal deposition near basement /cover unconformity: lessons and analogies from Pb-Zn-F-Ba systems for the understanding of Proterozoic U deposits. *Geofluids* 10: 270–292. <https://doi.org/10.1111/j.1468-8123.2010.00289.x>
- Bois C, Gariel O, Lefort J-P, Rolet J, Brunet M-F., Masse P. 1997. Geologic contribution of the Bay of Biscay deep seismic survey: a summary of the main scientific results, a discussion of the open questions and suggestions for further investigation. *Mém Société Géologique Fr* 171: 193–209.
- Bons PD, Elburg MA, Gomez-Rivas E. 2012. A review of the formation of tectonic veins and their microstructure. *J Struct Geol* 43: 33–62.
- Boutin A, de Saint Blanquat M, Poujol M, Boulvais P, de Parseval P, Rouleau C, *et al.* 2016. Succession of Permian and Mesozoic metasomatic events in the eastern Pyrenees with emphasis on the Trimouns talc-chlorite deposit. *Int J Earth Sci* 105: 747–770.
- Bouton P. 2004. Les grès à meules de Sérigné et de l'Hermenault en Vendée : matériau géologique et exploitation. *Le Naturaliste Vendéen* 4: 3–14.
- Bouton P, Branger P. 2007. Notice explicative, Carte géol. France (1/50000), feuille Coulonges-sur-l'Autize (587). Orléans: B.R.G.M.
- Bradley DC, Kidd WSF. 1991. Flexural extension of the upper continental crust in collisional foredeeps. *Geol Soc Am Bull* 103: 1416–1438.
- BRGM E-R., Esso-Rep S, 1974. Géologie du bassin d'Aquitaine. BRGM Editions.
- Brigaud B, Vincent B, Pagel M, Gras A, Noret A, Landrein P, *et al.* 2018. Sedimentary architecture, depositional facies and diagenetic response to intracratonic deformation and climate change inferred from outcrops for a pivotal period (Jurassic/Cretaceous boundary, Paris Basin, France). *Sediment Geol* 373: 48–76. <https://doi.org/10.1016/j.sedgeo.2018.04.011>
- Brown S, Allanic C, Brigaud B, Andrieu S, Mangenot X, Deloume-Carpentras Q, *et al.* 2021. Multiple phases of fracturation in Quercy (southwest France) limestones. Dating the stress record in an intraplate setting. In: *27e Réunion des Sciences de la Terre*, Lyon.
- B.S.S. n.d. BRGM database available at <https://infoterre.brgm.fr> (last consult : 2022/15/01)
- Burbaud-Vergneaud M. 1987. Fracturation et interactions socle-couverture : le seuil du Poitou. Données géologiques. Données de la télédétection infrarouge thermique. Poitiers: Université de Poitiers, pp. 202.

- Burisch M, Markl G, Gutzmer J. 2022. Breakup with benefits-hydrothermal mineral systems related to the disintegration of a supercontinent. *Earth Planet Sci Lett* 580: 117373.
- Cagnard F, Gapais D, Brun JP, Gumiaux C, Van den Driessche J. 2004. Late pervasive crustal-scale extension in the south Armorican Hercynian belt (Vendée, France). *J Struct Geol* 26: 435–449. <https://doi.org/10.1016/j.jsg.2003.08.006>
- Cathelineau M, Boiron M-C., Fourcade S, Ruffet G, Clauer N, Belcourt O, *et al.* 2012. A major Late Jurassic fluid event at the basin/basement unconformity in western France: 40Ar/39Ar and K-Ar dating, fluid chemistry, and related geodynamic context. *Chem Geol* 322-323: 99–120. <https://doi.org/10.1016/j.chemgeo.2012.06.008>
- Chew DM, Petrus JA, Kamber BS. 2014. U-Pb LA-ICP-MS dating using accessory mineral standards with variable common Pb. *Chem Geol* 363: 185–199. <https://doi.org/10.1016/j.chemgeo.2013.11.006>
- Clerc C, Lagabrielle Y, Labaume P, Ringenbach J-C., Vauchez A, Nalpas T. 2016. Basement-Cover decoupling and progressive exhumation of metamorphic sediments at hot rifted margin. Insights from the Northeastern Pyrenean analog. *Tectonophysics* 686: 82–97.
- Clerc C, Lagabrielle Y, Neumaier M, Reynaud J-Y., de Saint Blanquat M. 2012. Exhumation of subcontinental mantle rocks: evidence from ultramafic-bearing clastic deposits nearby the Lherz peridotite body, French Pyrenees. *Bull Soc Geol Fr* 183: 443–459.
- Cloetingh S, Burov E. 2011. Lithospheric folding and sedimentary basin evolution: a review and analysis of formation mechanisms. *Basin Res* 23: 257–290.
- Coltat R, Branquet Y, Gautier P, Campos Rodriguez H, Poujol M, Pelleter E, *et al.* 2019. Unravelling the root zone of ultramafic-hosted black smokers-like hydrothermalism from an Alpine analog. *Terra Nova* 31: 549–561.
- Cooper M. The analysis of fracture systems in subsurface thrust structure from the Foothills of the Canadian Rockies. In: McClay K, ed. *Thrust tectonics*. London: Chapman and Hall, 1992, pp. 217–233.
- Corre B, Boulvais P, Boiron M-C., Lagabrielle Y, Marasi L, Clerc C. 2018. Fluid circulations in response to mantle exhumation at the passive margin setting in the north Pyrenean zone, France. *Mineral Petrol* 112: 647–670.
- Curnelle R, Dubois P. 1986. Évolution mésozoïque des grands bassins sédimentaires français; bassins de Paris, d'Aquitaine et du Sud-Est. *Bull Soc Geol Fr* II: 529–546. <https://doi.org/10.2113/gssgfbull.II.4.529>
- Daubrée GA. 1878. Recherches expérimentales sur les cassures qui traversent l'écorce terrestre, particulièrement celles qui sont connues sous les noms de joints et de failles. *Comptes rendus des séances de l'Académie des sciences* 86: 283–289.
- De Ruig MJ. 1990. Fold trends and stress deviation in the Alicante fold belt, southeastern Spain. *Tectonophysics* 184: 393–403.
- DeFelipe I, Pedreira D, Pulgar JA, Iriarte E, Mendia M. 2017. Mantle exhumation and metamorphism in the Basque-Cantabrian Basin (N.S. Spain): stable and clumped isotope analysis in carbonates and comparison with opicalcites in the North-Pyrenean Zone (Urdach and Lherz). *Geochem Geophys Geosystems* 18: 631–652.
- Dennis JG. 1967. International tectonic dictionary. Tulsa: Am Assoc Pet. Geol. Mem 7.
- Dhifaoui R, Strzeczynski P, Mourgues R, Rigane A, Gourmelen C, Peigné D. 2021. Accommodation of compression and lateral extension in a continental crust: analogical modeling of the Central Atlas (eastern Algeria, Tunisia) and Pelagian sea. *Tectonophysics* 817: 229052. <https://doi.org/10.1016/j.tecto.2021.229052>.
- Dielforder A, Frasca G, Brune S, Ford M. 2019. Formation of the Iberian-European convergent plate boundary fault and its effect on intraplate deformation in Central Europe. *Geochem Geophys Geosystems* 20: 2395–2417.
- Doglionni C. 1995. Geological remarks on the relationships between extension and convergent geodynamic settings. *Tectonophysics* 252: 253–267.
- Ducoux M, Masini E, Tugend J, Gómez-Romeu J, Calassou S. 2021. Basement-decoupled hyperextension rifting: The tectono-stratigraphic record of the salt-rich Pyrenean necking zone (Arzacq Basin, SW France). *GSA Bull* 134: 941–964. <https://doi.org/10.1130/B35974.1>
- Duperret A, Vandycke S, Mortimore RN, Genter A. 2012. How plate tectonics is recorded in chalk deposits along the eastern English Channel in Normandy (France) and Sussex (U.K.). *Tectonophysics* 581: 163–181.
- Evans D, Graham C, Armour A, Bathurst P. 2003. The Millennium Atlas: petroleum geology of the central and northern North Sea. London: Geological Society of London.
- Fauré P, Bohain P. 2017. Les ammonites du Pliensbachien inférieur de la Vendée méridionale, France: étude taxonomique implications stratigraphiques et paléogéographiques, Strata. Lyon: Dédale éditions.
- François T, Barbarand J, Wyns R. 2020. Lower Cretaceous inversion of the European Variscan basement: record from the Vendée and Limousin (France). *Int J Earth Sci* 109: 1837–1852. <https://doi.org/10.1007/s00531-020-01875-z>
- Frizon de Lamotte D, Saint Bezar B, Bracène R, Mercier E. 2000. The two main steps of the Atlas building and geodynamics of the western Mediterranean. *Tectonics* 19: 740–761.
- Gapais D, Brun J-P., Gumiaux C, Cagnard F, Ruffet G, Le Carlier De Veslud C. 2015. Extensional tectonics in the Hercynian Armorican belt (France). An overview. *Bull Soc Geol Fr* 186: 117–129.
- Gerbault M, Burov EB, Poliakov AN, Daignières M. 1999. Do faults trigger folding in the lithosphere? *Geophys Res Lett* 26: 271–274.
- Gorczyk W, Hobbs B, Gessner K, Gerya T. 2013. Intra-cratonic geodynamics. *Gondwana Res* 24: 838–848.
- Goujou JC, Debrand-Passard S, Hantzpergue P, Le Bret P. 1994. Notice explicative, Carte géol. France (1/50000), feuille Les Sables d'Olonne-Longeville (584). Orléans: B.R.G.M.
- Granier B, Cougnon M, Bucur I, Prieur A. 2015. Redécouverte de la Tersella incompleta J. Morellet in J. Morellet & Ters, 1952. *Arch Sci* 68: 163–172
- Hancock PL. 1985. Brittle microtectonics: principles and practice. *J Struct Geol* 7: 437–457. [https://doi.org/10.1016/0191-8141\(85\)90048-3](https://doi.org/10.1016/0191-8141(85)90048-3)
- Horstwood MSA, Košler J, Gehrels G, Jackson SE, McLean NM Paton, *et al.* 2016. Community-derived standards for LA-ICP-MS U-(Th)-Pb geochronology – uncertainty propagation, age interpretation and data reporting. *Geostand Geoanal Res* 40 (3): 311–332.
- Huerta AD, Harry DL. 2007. The transition from diffuse to focused extension: modeled evolution of the West Antarctic Rift system. *Earth Planet Sci Lett* 255: 133–147.
- Huyghe D, Mouthereau F, Emmanuel L. 2012. Oxygen isotopes of marine mollusc shells record Eocene elevation change in the Pyrenees. *Earth Planet Sci Lett* 345-348: 131–141. <https://doi.org/10.1016/j.epsl.2012.06.035>
- Iglésias M, Brun J-P. 1976. Signification des variations et anomalies de la déformation dans un segment de la chaîne hercynienne (les séries cristallophylliennes de la Vendée littorale, Massif armoricain). *Bull Soc Geol Fr* 7: 1443–1452.
- Incerpi N, Manatschal G, Martire L, Bernasconi SM, Gerdes A, Bertok C. 2020. Characteristics and timing of hydrothermal fluid circulation in the fossil Pyrenean hyperextended rift system: new constraints from the Chaînons Béarnais (W Pyrenees). *Int J Earth Sci* 109: 1071–1093.

- Issautier B, Lasseur E, Saspiturry N, Angrand P, Andrieu S, Serrano O. 2022. Onset of Iberian-European plate convergence: Late Cretaceous flexural response of a hot lithosphere (Aquitaine Basin, France). *Tectonophysics* 843: 229504.
- Issautier B, Saspiturry N, Serrano O. 2020. Role of structural inheritance and salt tectonics in the formation of pseudosymmetric continental rifts on the European margin of the hyperextended Mauléon basin (Early Cretaceous Arzacq and Tartas Basins). *Mar Pet Geol* 118: 104395. <https://doi.org/10.1016/j.marpetgeo.2020.104395>
- Jammes S, Manatschal G, Lavier L, Masini E. 2009. Tectonosedimentary evolution related to extreme crustal thinning ahead of a propagating ocean: example of the western Pyrenees. *Tectonics* 28: TC4012.
- Jolivet L, Baudin T, Calassou S, Chevrot S, Ford M, Issautier B, *et al.* 2021. Geodynamic evolution of a wide plate boundary in the Western Mediterranean, near-field *versus* far-field interactions. *BSGF-Earth Sci Bull* 192: 48.
- Lacombe O. 2012. Do fault slip data inversions actually yield “paleostresses” that can be compared with contemporary stresses? A critical discussion. *Comptes Rendus Geosci* 344: 159–173.
- Lacombe O. 2010. Calcite twins, a tool for tectonic studies in thrust belts and stable orogenic forelands. *Oil Gas Sci Technol Revue d'IFP Energ Nouv* 65: 809–838.
- Lacombe O, Angelier J, Laurent P, Bergerat F, Tourneret C. 1990. Joint analyses of calcite twins and fault slips as a key for deciphering polyphase tectonics: burgundy as a case study. *Tectonophysics, Paleomagnetic Constraints on Crustal Motions* 182: 279–300. [https://doi.org/10.1016/0040-1951\(90\)90168-8](https://doi.org/10.1016/0040-1951(90)90168-8)
- Lacombe O, Mouthereau F. 1999. Qu'est-ce que le front des orogènes? L'exemple de l'orogène pyrénéen. *Comptes Rendus Académie Sci-Ser IIA-Earth Planet Sci* 329: 889–896.
- Lacombe O, Obert D. 2000. Héritage structural et déformation de couverture: plissement et fracturation tertiaires dans l'Ouest du bassin de Paris. *Comptes Rendus Académie Sci-Ser IIA-Earth Planet Sci* 330: 793–798.
- Lagabrielle Y, Asti R, Duret T, Clerc C, Fourcade S, Teixell A, *et al.* 2020. A review of cretaceous smooth-slopes extensional basins along the Iberia-Eurasia plate boundary: how pre-rift salt controls the modes of continental rifting and mantle exhumation. *Earth-Sci Rev* 201: 103071.
- Lagabrielle Y, Bodinier J-L. 2008. Submarine reworking of exhumed subcontinental mantle rocks: field evidence from the Lherz peridotites, French Pyrenees. *Terra Nova* 20: 11–21.
- Lagabrielle Y, Labaume P, de Saint Blanquat M. 2010. Mantle exhumation, crustal denudation, and gravity tectonics during Cretaceous rifting in the Pyrenean realm (S.W. Europe): insights from the geological setting of the lherzolite bodies. *Tectonics* 29: TC4012.
- Langhi L, Ciftci NB, Borel GD. 2011. Impact of lithospheric flexure on the evolution of shallow faults in the Timor foreland system. *Mar Geol* 284: 40–54.
- Leffondré P, Déverchère J, Medaouri M, Klingelhoefer F, Graindorge D, Arab M. 2021. Ongoing inversion of a passive margin: spatial variability of strain markers along the algerian margin and basin (Mediterranean Sea) and seismotectonic implications. *Front Earth Sci* 9.
- Manatschal G, Lavier L, Chenin P. 2015. The role of inheritance in structuring hyperextended rift systems: Some considerations based on observations and numerical modeling. *Gondwana Res* 27: 140–164. <https://doi.org/10.1016/j.gr.2014.08.006>
- McKenzie DP, Parker RL. 1967. The North Pacific: an example of tectonics on a sphere. *Nature* 216: 1276–1280.
- Missenard Y, Parizot O, Barbarand J. 2017. Age of the Fontainebleau sandstones: a tectonic point of view. *Bull Soc Geol Fr* 188 (4).
- Mouthereau F, Filleaudeau P-Y., Vacherat A, Pik R, Lacombe O, Fellin MG, *et al.* 2014. Placing limits to shortening evolution in the Pyrenees: role of margin architecture and implications for the Iberia/Europe convergence. *Tectonics* 33: 2283–2314.
- Munoz M, Baron S, Boucher A, Béziat D, Salvi S. 2016. Mesozoic vein-type Pb-Zn mineralization in the Pyrenees: Lead isotopic and fluid inclusion evidence from the Les Argentières and Lacore deposits. *Comptes Rendus Geosci* 348: 322–332.
- Navabpour P, Malz A, Kley J, Siegburg M, Kasch N, Ustaszewski K. 2017. Intraplate brittle deformation and states of paleostress constrained by fault kinematics in the central German platform. *Tectonophysics* 694: 146–163.
- Parizot O, Missenard Y, Barbarand J, Blaise T, Benedicto A, Haurine F, *et al.* 2022. How sensitive are intraplate inherited structure? Insight from the cévennes fault system (Languedoc, SE France). *Geol Mag*: 1–13.
- Parrish RR, Parrish CM, Lasalle S. 2018. Vein calcite dating reveals Pyrenean orogen as cause of Paleogene deformation in southern England. *J Geol Soc* 175: 425–442.
- Paton C, Hellstrom J, Paul B, Woodhead J, Hergt J. 2011. Iolite: freeware for the visualisation and processing of mass spectrometric data. *J Anal At Spectrom* 26: 2508–2518. <https://doi.org/10.1039/C1JA10172B>
- Peacock DCP, Nixon CW, Rotevatn A, Sanderson DJ, Zuluaga LF. 2016. Glossary of fault and other fracture networks. *J Struct Geol* 92: 12–29.
- Pollard DD, Aydin A. 1988. Progress in understanding jointing over the past century. *Geol Soc Am Bull* 100: 1181–1204.
- Quesnel B, Boiron M-C, Cathelineau M, Truche L, Rigaudier T, Bardoux G, *et al.* 2019. Nature and origin of mineralizing fluids in hyperextensional systems: the case of cretaceous Mg metasomatism in the Pyrenees. *Geofluids* 2019: 7213050.
- Roberts NMW, Holdsworth RE. 2022. Timescales of faulting through calcite geochronology: a review. *J Struct Geol* 158: 104578. <https://doi.org/10.1016/j.jsg.2022.104578>
- Roberts NMW, Rasbury ET, Parrish RR, Smith CJ, Horstwood MSA, Condon DJ. 2017. A calcite reference material for LA-ICP-MS U-Pb geochronology, *Geochem. Geophys Geosy* 18: 2807–2814. <https://doi.org/10.1002/2016gc006784>
- Rocher M, Lacombe O, Angelier J, Deffontaines B, Verdier F. 2000. Cenozoic folding and faulting in the south Aquitaine Basin (France): insights from combined structural and paleostress analyses. *J Struct Geol* 22: 627–645. [https://doi.org/10.1016/S0191-8141\(99\)00181-9](https://doi.org/10.1016/S0191-8141(99)00181-9)
- Roure F, Choukroune P, Berastegui X, Munoz JA, Villien A, Matheron P *et al.*, 1989. E.C.O.R.S. deep seismic data and balanced cross sections: geometric constraints on the evolution of the Pyrenees. *Tectonics* 8: 41–50.
- Salardon R, Carpentier C, Bellahsen N, Pironon J, France-Lanord C. 2017. Interactions between tectonics and fluid circulations in an inverted hyper-extended basin: Example of mesozoic carbonate rocks of the western North Pyrenean Zone (Chaînons Béarnais, France). *Mar Pet Geol* 80: 563–586.
- Sanderson DJ, Nixon CW. 2015. The use of topology in fracture network characterization. *J Struct Geol* 72: 55–66. <https://doi.org/10.1016/j.jsg.2015.01.005>
- Seymour NM, Stockli DF, Beltrando M, Smye AJ. 2016. Tracing the thermal evolution of the Corsican lower crust during Tethyan rifting. *Tectonics* 35: 2439–2466.
- Strzeczynski P, Dominguez S, Boudiaf A, Déverchère J. 2021. Tectonic inversion and geomorphic evolution of the algerian

- margin since messinian times: insights from new onshore/offshore analog modeling experiments. *Tectonics* 40: e2020TC006369. <https://doi.org/10.1029/2020TC006369>
- Strzeczynski P, Lenoir L, Bessin P, Bouat L. 2020. Brittle tectonics and fluids overpressure during the early stage of the Bay of Biscay opening in the Jard-sur-Mer area, (northern Aquitaine Basin, France). *Bull Soc Geol Fr* 191: 38. <https://doi.org/10.1051/bsgf/2020025>
- Szymanski E, Stockli DF, Johnson PR, Hager C. 2016. Thermo-chronometric evidence for diffuse extension and two-phase rifting within the Central Arabian Margin of the Red Sea Rift. *Tectonics* 35: 2863–2895.
- Tavani S, Storti F, Lacombe O, Corradetti A, Muñoz JA, Mazzoli S. *et al.*, 2015. A review of deformation pattern templates in foreland basin systems and fold-and-thrust belts: implications for the state of stress in the frontal regions of thrust wedges. *Earth-Sci Rev* 141: 82–104.
- Ters M, Gabilly J. 1986. Carte géol. France (1/50000), feuille Les Sables d'Olonne-Longeville (584). Orléans: B.R.G.M.
- Thomas G, Permanyer A, Delfaud J, Biteau J-J, Lagarigue J-L, Le Marrec A. 1996. Geometrie des depots de la formation de Lons (Kimmeridgien, bassin d'Aquitaine); interpretation structurale. *Bull Soc Geol Fr* 167: 627–636.
- Tugend J, Manatschal G, Kuszniir NJ. 2015. Spatial and temporal evolution of hyperextended rift systems: Implication for the nature, kinematics, and timing of the Iberian-European plate boundary. *Geology* 43: 15–18. <https://doi.org/10.1130/G36072.1>
- Tugend J, Manatschal G, Kuszniir NJ, Masini E, Mohn G, Thion I. . Formation and deformation of hyperextended rift systems: insights from rift domain mapping in the Bay of Biscay-Pyrenees. *Tectonics* 33: 1239–1276.
- Turcotte DL, Schubert G. 2002. *Geodynamics*, 2nd ed. Cambridge: Cambridge University Press. <https://doi.org/10.1017/CBO9780511807442>
- Turner JP, Williams GA. 2004. Sedimentary basin inversion and intra-plate shortening. *Earth-Sci Rev* 65: 277–304.
- Turrillot P, Augier R, Monié P, Faure M. 2011. Late orogenic exhumation of the Variscan high-grade units (South Armorican Domain, western France), combined structural and 40Ar/39Ar constraints. *Tectonics* 30: TC5007. <https://doi.org/10.1029/2010TC002788>
- Vergés J, Fernández M, Martínez A. 2002. The Pyrenean orogen: pre-, syn-, and post-collisional evolution. *J Virtual Explor* 8: 55–74.
- Vergés J, Millán H, Roca E, Muñoz JA, Marzo M, Cirés J *et al.*, 1995. Eastern Pyrenees and related foreland basins: pre-, syn- and post-collisional crustal-scale cross-sections. *Mar Pet Geol* 12: 903–915.
- Vermeesch P. 2018. IsoplotR: A free and open tool box for geochronology. *Geosci Front* 9: 1479–1493. <https://doi.org/10.1016/j.gsf.2018.04.001>
- Virgo S, Abe S, Urai JL. 2014. The evolution of crack seal vein and fracture networks in an evolving stress field: insights from discrete element models of fracture sealing. *J Geophys Res Solid Earth* 119: 8708–8727. <https://doi.org/10.1002/2014JB011520>
- Ziegler PA. 1990. *Geological Atlas of Western and Central Europe*, 2nd Edition. London: Shell Internationale Petroleum Mij. B.V. and Geological Society.
- Ziegler PA, Cloetingh S, van Wees J-D. 1995. Dynamics of intra-plate compressional deformation: the Alpine foreland and other examples. *Tectonophysics* 252: 7–59.
- Ziegler PA, Dèzes P. 2005. Evolution of the lithosphere in the area of the Rhine Rift System. *Int J Earth Sci (Geol Rundsch)* 94: 594–614. <https://doi.org/10.1007/s00531-005-0474-3>

**Cite this article as:** Bouat L, Strzeczynski P, Mourgues R, Branquet Y, Cogné N, Barré G, Gardien V. 2023. Early, far-field and diffuse tectonics records in the North Aquitaine Basin (France), *BSGF - Earth Sciences Bulletin* 194: 17.